

1  
2  
3  
4  
5  
6  
7  
8  
9  
10  
11  
12  
13  
14  
15  
16  
17  
18  
19  
20  
21  
22  
23  
24  
25  
26  
27  
28

**Petrogenesis of Luchaba and Wuchaba granitoids in Western Qinling: geochronological and geochemical evidence**

Juanjuan Kong <sup>a, b, c, \*</sup>, Yaoling Niu <sup>a, b, d, \*</sup>, Meng Duan <sup>e</sup>, Yu Zhang <sup>f</sup>, Yan Hu <sup>a</sup>, Jiyong Li <sup>a, b, c</sup>, Shuo Chen <sup>a, b, c</sup>

<sup>a</sup> Institute of Oceanology, Chinese Academy of Sciences, Qingdao 266071, China

<sup>b</sup> Laboratory for Marine Geology, Qingdao National Laboratory for Marine Science and Technology, Qingdao 266061, China

<sup>c</sup> University of Chinese Academy of Sciences, Beijing 100049, China

<sup>d</sup> Department of Earth Sciences, Durham University, Durham DH1 3LE, UK

<sup>e</sup> School of Earth Science and Resources, China University of Geosciences, Beijing 100083, China

<sup>f</sup> School of Earth Sciences, Lanzhou University, Lanzhou 730000, China

\*Corresponding authors:

Miss Juanjuan Kong, [juanjuan0317@foxmail.com](mailto:juanjuan0317@foxmail.com)

Professor Yaoling Niu, [yaoling.niu@foxmail.com](mailto:yaoling.niu@foxmail.com)

Address: Institute of Oceanology, Chinese Academy of Sciences, No. 7 Nanhai Road, Shinan District, Qingdao 266071, China. Tel.: +86 0532 82898980

29 Abstract

30 The West Qinling Orogenic Belt (WQOB) is a major portion of the Qinling-Dabie-Sulu  
31 Orogen and holds essential information for understanding the prolonged evolution of the  
32 northeastern branch of the Paleo-Tethys in East Asia. This study focuses on the petrogenesis  
33 of granitoids from Luchuba and Wuchaba plutons in the WQOB. We obtained zircon U-Pb ages  
34 of  $211 \pm 1.4$ Ma for the Luchuba pluton and  $218.7 \pm 1.3$ Ma for the Wuchaba pluton, which are  
35 the same as the proposed timing of continental collision at  $\sim 220$ Ma. We thus interpret the  
36 granitoids to represent a magmatic response to the collision between the North China Craton  
37 (NCC) and the Yangtze Block (YB). The two plutons are metaluminous to weakly  
38 peraluminous I-type granitoids. Samples from the two plutons show strong light rare earth  
39 element (REEs) enrichment and weak heavy REE depletion, with varying negative Eu  
40 anomalies, which is most consistent with significant plagioclase fractionation although the  
41 possible effect of plagioclase as residual phase in the magma source region cannot be ruled out.  
42 In primitive mantle normalized multi-element variation diagrams, nearly all the samples show  
43 negative Nb, Ta, P and Ti anomalies and relative enrichment in Rb, Pb, U and K. These  
44 characteristics resemble those of the average continental crust. The Luchuba pluton has lower  
45  $(^{87}\text{Sr}/^{86}\text{Sr})_i$  (0.7051 to 0.7104), higher  $\epsilon_{\text{Nd}}(t)$  (-8.11 to -5.73) and  $\epsilon_{\text{Hf}}(t)$  (-6.70 to -1.65) than  
46 mature continental crust ( $[(^{87}\text{Sr}/^{86}\text{Sr})_i > 0.72, \epsilon_{\text{Nd}}(t) < -12]$ ). The Wuchaba pluton also has lower  
47  $(^{87}\text{Sr}/^{86}\text{Sr})_i$  (0.7069 to 0.7080), higher  $\epsilon_{\text{Nd}}(t)$  (-9.86 to -3.34) and  $\epsilon_{\text{Hf}}(t)$  (-5.69 to 1.58) than  
48 mature continental crust. We conclude that the Luchuba and Wuchaba granitoids in the WQOB  
49 are best explained as resulting from fractional crystallization with crustal assimilation of  
50 parental magmas derived from melting of Mianlue oceanic crust under amphibolite facies  
51 conditions during the initial stage of continental collision between the North China Craton and  
52 the Yangtze Block. Mafic magmatic enclaves (MMEs) of Wuchaba pluton are earlier  
53 cumulates of the same magmatic system. The Mianlue oceanic crust (MORB-like) contributes  
54 to the source of the Luchuba and Wuchaba granitoids, pointing to the significance of melting  
55 of oceanic crust for continental crust accretion.

56 ***Key words:*** Western Qinling; Luchuba and Wuchaba granitoids; granitoid petrogenesis; crust  
57 accretion.

## 58 **Introduction**

59 The Qinling Orogen is one of the largest orogenic belts in Asia (Mattauer et al. 1985), linking  
60 Kunlun and Qilian orogens to the west and Dabie–Sulu orogen to the east (Meng and Zhang  
61 2000; Ratschbacher et al. 2003), across Central China for ~ 2500 km. It developed through a  
62 series of complex seafloor subduction and terrane collision events (Zhang et al. 2001;  
63 Ratschbacher et al. 2003; Wang et al. 2009; Wu and Zheng 2012), ultimately completed as the  
64 result of the continental collision between the Yangtze Block (YB) and the North China Craton  
65 (NCC) along the Mianlue suture zone in the early Mesozoic (see Fig. 1; Dong et al. 2011 and  
66 references therein). Abundant granitoids throughout much of the West Qinling were produced  
67 during this time period and have received much attention in recent years with mounting  
68 geochronological and geochemical data with the aim of better understanding magma sources  
69 and processes in the context of studying the Qinling orogenesis. However, the petrogenesis of  
70 these granitoids remains controversial (Sun et al. 2002a, b; Wang et al. 2007, 2011; Qin et al.  
71 2009, 2010; Liu et al. 2011a, b; Dong et al. 2011, 2012; Yang et al. 2011, 2012; Xiao et al.  
72 2013), and the debate mainly centers on the sources of these granitoids (e.g., upper crust, lower  
73 crust or crust-mantle magma mixing) and the geodynamic evolution.

74 In this paper, we focus on the Luchaba and Wuchaba granitoid plutons in the central West  
75 Qinling Orogenic Belt (WQOB) because of the geological information available due to the  
76 associated mineralization and its exploration. Existing models on the petrogenesis of these  
77 plutons include: (1) upper crust melting (Ou et al. 2010; Peng 2012, 2013); (2) lower crust  
78 melting (Xu et al. 2013); (3) partial melting of Mesoproterozoic crustal rocks and melt

79 interaction with sub-continental lithospheric mantle (SCLM) (the interpreted source of MMEs)  
80 (Zhu et al. 2013). The crystallization age of the Wuchaba pluton has been hotly debated to vary  
81 from 264 to 213 Ma (Gao et al. 2011; Li et al. 2012; Peng 2012, 2013; Xu et al. 2014; Zeng et  
82 al. 2014; Wang et al. 2015) for multi-stage magmatic emplacement with views on tectonic  
83 settings varying from subduction-related, syn-collisional to post-collisional (Lu 2004; Li et al.  
84 2012). Debates on the petrogenesis and tectonic settings of the Luchuba and Wuchaba  
85 granitoids continued. It should be noted that previous studies on the Luchuba and Wuchaba  
86 plutons are limited with little systemic chronology, geochemistry and isotopic data. Here we  
87 present new LA-ICP-MS zircon U-Pb ages, bulk-rock major and trace element data and Sr–  
88 Nd–Hf isotopic compositions to discuss the petrogenesis of these two granitoid plutons in the  
89 context of geodynamic evolution.

#### 90 **Geological setting and samples**

91 The Qinling orogenic belt is adjacent to the Qilian orogenic belt (Fig. 1a) and is bounded by  
92 the Linxia–Wushan–Tianshui fault to the north and the Mianlue suture in the south (Fig. 1b).  
93 The Qinling orogen has been divided into East and West Qinling on the basis of their geological  
94 differences (Zhang et al. 2001, 2005, 2007; Feng et al. 2002) (Fig. 1b). The granitoids with  
95 ages of 245–200 Ma are distributed between the Shangdan and Mianlue sutures along an  
96 approximately E-W trending zone (Zhu et al. 2011; Dong et al. 2011). The WQOB is interpreted  
97 as having undergone supercontinent breakup, Qinling-Qilian-Kunlun seafloor spreading and  
98 subduction, continent-continent collision and intraplate processes since the Neoproterozoic  
99 (Xu et al. 2014).

100 In the WQOB, the Phanerozoic strata are mostly Devonian-Cretaceous sedimentary units

101 with minor Cambrian-Silurian sedimentary units. The Precambrian basement is rarely exposed  
102 (Feng et al. 2002). Zhang et al. (2007) confirm that the basement of the WQOB has affinities  
103 with the Yangtze block. The Luchuba pluton crops out over an area of  $\sim 117$  km<sup>2</sup>, intruding  
104 Devonian and Carboniferous limestone, sandstone and shale (Ou et al. 2010). The Wuchaba  
105 pluton, also known as Zhongchuan pluton, has a circular shape with an outcrop area of  $\sim 210$   
106 km<sup>2</sup> (Zeng et al. 2012), intruding the Middle Devonian Shujiaba group (D2sh<sup>1</sup>) and  
107 Carboniferous Xiajialing group (C1x) (Fig. 1c). In the field, the Luchuba granitoids are light  
108 grey, and structurally massive with medium-grained or porphyritic texture (Fig. 2a). The  
109 Wuchaba granitoids (Fig. 2b) are light red and smoky gray in color, with medium-to coarse-  
110 grained and porphyritic texture. Mafic magmatic enclaves (MMEs) occur locally in both  
111 Luchuba and Wuchaba plutons, exhibit angular to oval shapes and varying size (10 to 20 cm  
112 in diameter), and have no chilled margins with the host granitoids (Fig. 2a, b).

113 The Luchuba granitoids are mainly composed of granodiorite (Fig. 3a) and biotite  
114 monzogranite (Fig. 3b), and have porphyritic texture with the mineral assemblage of  
115 plagioclase ( $\sim 30$  to  $40\%$ ) + K-feldspar ( $\sim 10$  to  $20\%$ ) + quartz ( $\sim 30$  to  $40\%$ ) with total biotite +  
116 hornblende ( $\sim 5$  to  $10\%$ ). The Wuchaba pluton mainly includes biotite monzogranite (Fig. 3c),  
117 biotite granite and diorite with the mineral assemblage similar to that of the Luchuba pluton.  
118 The mineralogy is dominantly plagioclase ( $\sim 30\%$ ), quartz ( $\sim 20\%$ ), K-feldspar ( $\sim 30$  to  $40\%$ )  
119 with minor hornblende and biotite ( $\sim 10\%$  in total) and accessory minerals such as apatite,  
120 zircon and Fe-Ti oxides. The MMEs are fine-grained and show equigranular and  
121 hypidiomorphic textures. It is important to note that the MMEs share the same mineralogy with  
122 the more felsic hosts but have greater modes of mafic minerals ( $\sim 55\%$  hornblende and biotite)

123 and lesser plagioclase (~20%), quartz (~10%) and K-feldspar (~10%) (Fig. 3d and Fig. 3e).  
124 Acicular apatite is ubiquitous in the MMEs (Fig. 3f). Euhedral to subhedral plagioclase crystals  
125 occur either as phenocrysts or as elongate laths. Quartz commonly occurs as anhedral grains.  
126 K-feldspar is mainly megacrysts. Apatite and hornblende display euhedral habit.

## 127 **Analytical methods**

128 In this study, 24 representative samples (including 2 host-MME pairs) from the Luchuba and  
129 Wuchaba plutons were analyzed for whole-rock major and trace elements, three of these  
130 representative samples were selected for zircon U-Pb dating. Fifteen of these samples were  
131 analyzed for whole-rock Sr-Nd-Hf isotope compositions. Weathered surfaces were removed  
132 and thoroughly cleaned, then ultrasonically cleaned with Milli-Q water and dried before the  
133 material was powdered to less than 200-mesh in a clean environment using an agate mill for  
134 analysis.

### 135 *LA-ICP-MS zircon U-Pb dating*

136 Zirconium were extracted using combined techniques of heavy liquid and magnetic separation.  
137 The zircon internal structure was examined using cathodoluminescence (CL) imaging on an  
138 EMPA-JXA-8100 scanning electron microscope at China University of Geosciences, Wuhan  
139 (CUGW) (Fig. 4). Zircon U-Pb dating on samples SEB12-01, YDB12-05 and DPC12-01 was  
140 carried out at the Geologic Lab Center, China University of Geosciences, Beijing (CUGB)  
141 using an Agilent 7500a inductively coupled plasma mass spectrometer (ICP-MS) with New  
142 Wave UPP-193 laser ablation system. During the analysis, laser spot size was set to ~36  $\mu\text{m}$   
143 for most analyses and to 25  $\mu\text{m}$  for metamorphic rims with laser energy density set at 8.5  $\text{J}/\text{cm}^2$   
144 and repetition rate at 10 Hz. The procedure of laser sampling is 5s pre-ablation, 20s sample-

145 chamber flushing and 40s sampling ablation. The ablated material is carried into the ICP-MS  
146 by the high-purity Helium gas stream with a flux of 0.8 L/min. The whole laser path was fluxed  
147 with N<sub>2</sub> (15 L/min) and Ar (1.15 L/min) in order to increase energy stability. The counting time  
148 for U, Th, <sup>204</sup>Pb, <sup>206</sup>Pb, <sup>207</sup>Pb and <sup>208</sup>Pb is 20 ms, and is 15 ms for other elements. Calibrations  
149 for the zircon analyses were carried out using NIST 610 as an external standard and Si as  
150 internal standard. U-Pb isotope fractionation effects were corrected for using zircon 91500  
151 (Wiedenbeck et al. 1995) as external standard. The data were processed using the  
152 GLITTER4.41 program with common Pb correction done following Andersen (2002) and  
153 analytical details described in Song et al. (2010a). The age data are given in Table 2 and the  
154 concordia diagrams and weighted mean age calculations were done using ISOPLOT 4.15  
155 (Ludwig 2012; Fig. 5).

#### 156 *Major and trace elements*

157 Whole-rock major and trace elements were analyzed using Prodigy Inductively Coupled  
158 Plasma Optical Emission Spectrometer (ICP-OES) and Agilent 7500a ICP-MS, respectively at  
159 CUGB. Analyses of United States Geological Survey (USGS) rock standards (AGV-2 and  
160 GSR-1) and Chinese national rock standard (GSR-3) give precision and accuracy better than  
161 5% (2σ) for major elements and 10% (2σ) for trace elements. Analytical details are given in  
162 Song et al. (2010b).

#### 163 *Sr–Nd–Hf isotopes*

164 For Sr, Nd and Hf isotope analyses, about 100 mg of sample powder was dissolved in a HF +  
165 HNO<sub>3</sub> mixture in Teflon beakers. The Sr, Nd and Hf were then separated using cation-exchange  
166 techniques. The Sr isotope ratios were measured using a Finnigan Triton Thermal Ionization



167 Mass Spectrometer (TIMS) and the Hf and Nd isotope ratios were measured using Multi-  
168 Collector Inductively Coupled Plasma Mass Spectrometry (MC-ICP-MS) at Guangzhou  
169 Institute of Geochemistry. The  $^{87}\text{Sr}/^{86}\text{Sr}$ ,  $^{143}\text{Nd}/^{144}\text{Nd}$  and  $^{176}\text{Hf}/^{177}\text{Hf}$  ratios are reported as  
170 values normalized to  $^{86}\text{Sr}/^{88}\text{Sr}$  of 0.1194,  $^{146}\text{Nd}/^{144}\text{Nd}$  of 0.7219 and  $^{179}\text{Hf}/^{177}\text{Hf}$  of 0.7325,  
171 respectively. During our analysis, repeated analyses of the NBS-987 Sr standard yielded  
172  $^{87}\text{Sr}/^{86}\text{Sr} = 0.710287 \pm 20$  ( $n = 21, 2\sigma$ ) and JNdi-1 Nd standard gave  $^{143}\text{Nd}/^{144}\text{Nd} 0.512086 \pm$   
173  $16$  ( $n = 11, 2\sigma$ ). Analyses of Hf standard yielded  $^{176}\text{Hf}/^{177}\text{Hf}$  of  $0.283099 \pm 15$  ( $n = 13, 2\sigma$ ) for  
174 BHVO-2 and  $0.283216 \pm 15$  ( $n = 6, 2\sigma$ ) for JB-3, which are consistent with the reference values  
175 (Raczek et al. 2003, Li et al. 2010). Sample preparation procedures and analytical details are  
176 described in Wei et al. (2002) and Li et al. (2004, 2005).

## 177 **Results**

### 178 *Zircon U–Pb data*

179 Zircon cathodoluminescence (CL) images are shown in Fig. 4. Most zircons are euhedral with  
180 oscillatory or linear zoning, ranging from 100 to 300 $\mu\text{m}$  in length with variable Th (65 to 805  
181 ppm), U (175 to 3300 ppm) and Th/U ratio (0.058 to 1.04), which is consistent with a magmatic  
182 origin (Rubatto and Gebauer 2000; Corfu et al. 2003; Hanchar and Hoskin 2003; Cao et al.  
183 2011).

184 Thirty grains of zircon from sample SEB12-01 of the Luchuba pluton were analyzed  
185 (Table 1). Three spots were excluded in the age calculation because of their high  $^{204}\text{Pb}$  and  
186 significant deviation from the concordia. Twenty-seven spots form a cluster giving a weighted  
187 mean  $^{206}\text{Pb}/^{238}\text{U}$  age of  $211 \pm 1.4$  Ma (MSWD = 1.4,  $n = 27$ ) (Fig. 5a). All the 24 zircon grains  
188 from sample YDB12-05 of the Luchuba pluton plot close to the concordia curve (Fig. 5b). Two

189 grains give younger ages of 195 Ma and 196 Ma probably due to Pb loss. Other grains give a  
190 weighted mean  $^{206}\text{Pb}/^{238}\text{U}$  age of  $218.5 \pm 2.3\text{Ma}$  (MSWD = 2.9, n = 22). Twenty zircons from  
191 sample DPC12-01 of the Wuchaba pluton give a weighted mean  $^{206}\text{Pb}/^{238}\text{U}$  age of  $218.3 \pm$   
192  $1.7\text{Ma}$  (MSWD = 0.56, n = 20) (Fig. 5c). All these are interpreted as crystallization ages of the  
193 two plutons. The two distinct ages of  $211 \pm 1.4\text{Ma}$  and  $218.5 \pm 2.3\text{Ma}$  of the Luchuba pluton  
194 suggests prolonged magmatism during the same event.

### 195 *Major and trace elements*

196 Whole-rock major and trace element compositions of the granitoids and MMEs from the  
197 Luchuba and Wuchaba plutons are given in Table 2. The Luchuba granitoids show varying  $\text{SiO}_2$   
198 (64.15 to 75.82wt.%) as do the Wuchaba granitoids (64.61 to 73.91wt.%  $\text{SiO}_2$ ). In the  $\text{K}_2\text{O} +$   
199  $\text{Na}_2\text{O}$  vs.  $\text{SiO}_2$  diagram (Fig. 6), most of the samples from the Luchuba and Wuchaba granitoids  
200 display a roughly continuous compositional spectrum from granodiorite to granite in  
201 subalkaline field with aluminum saturation index ( $[\text{ASI} = \text{molar Al}_2\text{O}_3 / (\text{CaO} + \text{K}_2\text{O} + \text{Na}_2\text{O})]$ )  
202  $\leq 1.10$  (Fig. 7). They exhibit a high K character with high  $\text{K}_2\text{O}/\text{Na}_2\text{O}$  (1.02 to 1.32 for Luchuba  
203 and 1.11 to 2.28 for Wuchaba plutons, Table 3). The high  $\text{K}_2\text{O}$  sample (MZG12-02) has high  
204 modal biotite and K-feldspar (~30%), while the low  $\text{K}_2\text{O}$  sample (CJM12-01(host)) has few  
205 modal biotite and K-feldspar (< 5%). In  $\text{SiO}_2$  variation diagrams (Fig. 8), most samples from  
206 the two plutons define a roughly correlated evolution trend:  $\text{Al}_2\text{O}_3$ ,  $\text{CaO}$ ,  $\text{Fe}_2\text{O}_3$ ,  $\text{MgO}$ ,  $\text{TiO}_2$ ,  
207  $\text{P}_2\text{O}_5$ , Sr, Eu and Yb decrease with increasing  $\text{SiO}_2$  whereas  $\text{Na}_2\text{O}$  and  $\text{K}_2\text{O}$  increase with  
208 increasing  $\text{SiO}_2$ . The Luchuba granitoids display strongly fractionated REE patterns ( $(\text{La}/\text{Yb})_{\text{N}}$   
209 = 5.28 to 18.84) with moderately negative Eu anomalies ( $\text{Eu}/\text{Eu}^* = 0.41$  to 0.83) (Fig. 9a). The  
210 Wuchaba granitoids show moderate to strong LREE enrichment ( $(\text{La}/\text{Yb})_{\text{N}} = 4.13$  to 34.61) and

211 variable negative Eu anomalies ( $\text{Eu}/\text{Eu}^* = 0.16$  to  $0.86$ ; Fig. 9c). Samples from the Luchuba  
212 and Wuchaba plutons have low Sr content and significant negative Sr anomalies ( $\text{Sr}/\text{Sr}^* =$   
213  $2\text{Sr}_N/[\text{Pr}_N + \text{Nd}_N]$ ), corresponding to its significant negative Eu anomalies (Fig. 10), which is  
214 most consistent with significant plagioclase fractionation although the possible effect of  
215 plagioclase as residual phase in the magma source region cannot be ruled out. In the trace  
216 element spider diagrams, all the samples show negative Nb, Ta, P and Ti anomalies and Rb, Th,  
217 U and K enrichment (Fig. 9b, d). These characteristics resemble those of bulk continental crust  
218 (BCC; Rudnick and Gao 2003).

219 The MMEs from the Wuchaba pluton have relatively lower  $\text{SiO}_2$  contents (53.31 and  
220 53.92 wt.%; Figs. 6, 8) and show the same composition in the TAS diagram (Fig. 6). The MMEs  
221 have negative Eu anomalies with  $\text{Eu}/\text{Eu}^*$  of 0.26 and 0.65, displaying higher abundances of  
222 HREEs (Fig. 9c) and higher Nb/Ta (17.52 and 17.38) than the host, which is consistent with  
223 higher modal contents of hornblende (Foley et al. 2000; Niu and O'Hara 2009; Chen et al. 2015,  
224 2016).

#### 225 *Sr-Nd-Hf isotopes*

226 Whole rock Sr-Nd-Hf isotope data for 15 samples (including two MMEs) of the two plutons  
227 are given in Table 3 and plotted in Figs. 11-13. The  $I_{\text{Sr}}(t)$ ,  $\epsilon_{\text{Nd}}(t)$  and  $\epsilon_{\text{Hf}}(t)$  refer to the age ( $t =$   
228 220 Ma) corrected values. All the analyzed Luchuba samples have variable values of  $I_{\text{Sr}}(t)$   
229 (0.7052 to 0.7104),  $\epsilon_{\text{Nd}}(t)$  of -8.11 to -5.73 and  $\epsilon_{\text{Hf}}(t)$  of -6.70 to -1.65. The Wuchaba pluton has  
230 the isotopic characteristics of  $I_{\text{Sr}}(t) = 0.7069$  to  $0.7080$ ,  $\epsilon_{\text{Nd}}(t) = -9.86$  to  $-3.34$  and  $\epsilon_{\text{Hf}}(t) = -5.69$   
231 to  $1.58$ . The two MMEs of Wuchaba granitoids also show Sr-Nd-Hf isotopic compositions ( $I_{\text{Sr}}(t)$   
232 is  $0.7069$  and  $0.7073$ ,  $\epsilon_{\text{Nd}}(t) = -4.74$  and  $-3.34$ ,  $\epsilon_{\text{Hf}}(t) = -0.78$  and  $1.58$ ) comparable to those of

233 Wuchaba host. Sample ZKL12-01 of the Luchuba pluton gives very high  $^{87}\text{Sr}/^{86}\text{Sr}$  of 0.737981.  
234 This high ratio is consistent with the high Rb/Sr ratio resulting from significant extent of  
235 plagioclase-dominated fractional crystallization (also low in Ba, P, and Ti; see Fig. 9). The high  
236  $^{87}\text{Rb}/^{86}\text{Sr}$  ratio (10.50) makes the calculated  $I_{\text{Sr}}(t)$  unreliable (Jahn et al. 2000).

## 237 **Discussion**

### 238 *Assimilation and Fractional crystallization (AFC)*

239 The data shown in  $\text{SiO}_2$ -variation diagrams (Fig. 8) are to a first-order consistent with varying  
240 extent of fractional crystallization of hornblende, plagioclase, Fe–Ti oxides and apatite.  
241 However, these trends are also consistent with modal variations of these phases in the samples  
242 although the depletion in P, Nb, Ta and Ti emphasizes the significance of fractional  
243 crystallization. These granitoids display sub-chondritic Nb/Ta ratio, which is also consistent  
244 with hornblende controlled fractionation ( $K_d_{\text{hornblende Nb/Ta}} = 1.40$ ) (Foley et al. 2002). The  
245 moderately to strongly negative anomalies of Ba, Sr and Eu (Fig. 9 and Fig. 10) indicate  
246 extensive fractionation of plagioclase and/or K-feldspar (Wu et al. 2003). The scattered data in  
247 the  $I_{\text{Sr}}$  vs.  $1/\text{Sr}$  and  $\epsilon_{\text{Nd}}(t)$  vs.  $1/\text{Nd}$  plots (Fig. 11) suggest that the petrogenesis of samples from  
248 the two plutons was controlled by fractional crystallization and contamination (Xing et al.  
249 1996). While scattered, it is apparent in Fig. 12 that the two plutons show quite similar range  
250 of initial  $^{87}\text{Sr}/^{86}\text{Sr}$  values (except for sample ZKL12-01 with high Rb/Sr) while the  $\epsilon_{\text{Nd}}(t)$  and  
251  $\epsilon_{\text{Hf}}(t)$  values decrease with increasing  $\text{SiO}_2$ , which is consistent with fractional crystallization,  
252 accompanied by increased crustal contamination/assimilation. It should be noted that the  
253 small variation of Sr isotopes reflects similar Sr isotope composition of the actually  
254 contaminated crust. All these data signify that assimilation–fractional crystallization (AFC)

255 processes (DePaolo 1981) played a role in the petrogenesis of the two plutons.

### 256 *Petrogenesis of granitoids*

257 Generally, granitoids are typically divided into I-, S-, A- and M-type in terms of source rock  
258 types and petrogenesis (e.g., Chappell et al. 1974; Collins et al. 1982; Whalen 1985).  
259 Amphibole, cordierite, and alkaline minerals are important diagnostic minerals for  
260 discriminating I-, S- and A-type granites respectively. The absence of aluminous minerals such  
261 as muscovite, tourmaline and garnet, combined with the magmatic assemblage of hornblende  
262 and biotite (Fig. 3), and the relatively low A/CNK values ( $\leq 1.1$ , Fig. 7) is consistent with  
263 these granitoids being of I-type.

264 The Luchuba and Wuchaba plutons have low  $(La/Yb)_N$  and Sr/Y, suggesting that their  
265 parental magmas were generated under relatively low pressures ( $\sim 40$  km) without garnet being  
266 present as the residual phase in the magma source region or as liquidus phase during magma  
267 evolution (e.g., Martin et al. 2005; Klein et al. 2000; Pertermann et al. 2004). Here we  
268 emphasize a maximum depth of  $\sim 40$  km for melt formation because of the lack of garnet  
269 signature in the two granitoid plutons (Mo et al. 2008).

270 Partial melting of the lower continental crust may account for the origin of granitic rocks,  
271 and some authors argued that the magma sources for the WQOB granitoids could be basic  
272 rocks (amphibolite) (Zhang et al. 2007). However, the dehydration melting of amphibolite in  
273 the lower crust should result in melts high in  $Na_2O$  and low in  $K_2O$  (Beard and Lofgren 1991),  
274 which is inconsistent with the high-K characteristics of the Luchuba and Wuchaba plutons.  
275 Besides, partial melting of the basaltic source usually needs higher melting temperature and  
276 amphibole dehydration melting cannot produce such volumetrically significant granitoids.

277 Thus, the origin by partial melting of pre-existing mafic lower crust is less likely. The Luchuba  
278 and Wuchaba plutons, as other coeval granites elsewhere in the WQOB, have lower ( $^{87}\text{Sr}/^{86}\text{Sr}$ )<sub>i</sub>,  
279 higher  $\epsilon_{\text{Nd}}(t)$  and  $\epsilon_{\text{Hf}}(t)$  than the mature continental crust ( $[\text{Sr}/^{86}\text{Sr}]_i > 0.72$ ,  $\epsilon_{\text{Nd}}(t) < -12$ ) (Fig.  
280 13a) (Zhang et al. 2007). Hence, it is unlikely that these granitoids were produced by melting  
281 of mature continental crust (upper crust) ( $[\text{Sr}/^{86}\text{Sr}]_i > 0.72$ ,  $\epsilon_{\text{Nd}}(t) < -12$ ) (Niu et al. 2009), but  
282 has significant mantle contribution (or juvenile crustal material) in terms of isotopes. In  
283 addition, Hf-Nd isotopes are coupled and lie in the global mantle and crustal array (Fig. 13b)  
284 indicating mantle (or juvenile continental crust) contribution. In the age- $\epsilon_{\text{Hf}}(t)$  diagram (Fig.  
285 13c), the majority of samples fall between the mantle and crustal evolution line, also indicating  
286 significant mantle contribution for these granitoids (Wang et al. 2012). Additionally, pioneering  
287 studies (Dong et al. 2011, 2012) suggest that the Paleo-Tethys Mianlue Ocean was already  
288 closed at the time of granitoids emplacement ( $\sim 220\text{Ma}$ ). Therefore, we suggest that the  
289 Luchuba and Wuchaba plutonism was a response to continental collision. In the context of  
290 continental collision, reasonable mechanism for granitoid magmatism with significant mantle  
291 isotopic signature was discussed by Niu et al. (2013). Partial melting of subducted basaltic  
292 ocean crust (Mianlue MORB) under amphibolite facies conditions can produce andesitic melts  
293 resembling bulk continental crust (BCC) (Niu et al. 2013; also see below). Note that the lack  
294 of adakite signature (i.e., high Sr/Y and La/Yb; Defant and Drummond 1990; Castillo 2006  
295 2012) requires melting under amphibolite facies conditions (see Niu et al. 2013). In this study,  
296 the Luchuba and Wuchaba plutons have REE and trace element patterns resembling those of  
297 the BCC (Fig. 9). Despite the felsic compositions with radiogenic Sr and unradiogenic Nd of  
298 the Luchuba and Wuchaba plutons, they have higher  $\epsilon_{\text{Nd}}(t)$  value than typical continental crust,

299 especially their high  $\epsilon_{\text{Hf}}(t)$  values are close to zero (see above). Simple isotopic mixing  
300 calculations suggest that  $\sim 50\%$  ocean crust (MORB) contributes to the source of the Luchuba  
301 and Wuchaba plutons (Fig. 14). Hence, the syncollisional plutons represent juvenile crust with  
302 primary materials isotopically coming from the mantle. In this case, the remaining part of the  
303 Mianlue oceanic crust is most likely the best source for generating andesitic magmas parental  
304 to the Luchuba and Wuchaba plutons; partial melting of the basaltic oceanic crust produces  
305 felsic melts and the ocean crust derived from the mantle not long ago imparts the mantle  
306 isotopic signature (Niu et al. 2013). Meanwhile, AFC during magma ascent can explain the  
307 crustal signatures of the Luchuba and Wuchaba granitoids.

#### 308 *Origin of MMEs*

309 Both Luchuba and Wuchaba plutons contain mafic magmatic enclaves (MMEs). The origin of  
310 the MMEs is key to the petrogenesis of the granitoids. Three models have been proposed to  
311 explain the origin of MMEs: (1) restites (Chen et al. 1989; Chappell et al. 2000); (2)  
312 representing mantle derived melts (Barbarin 2005; Mo et al. 2007; Yang et al. 2007; Clemens  
313 and Stevens 2011); (3) mafic cumulate of the same magmatic system with the host (Wall et al.  
314 1987; Dahlquist 2002; Niu et al. 2013; Huang et al. 2014; Chen et al. 2015, 2016). The MMEs  
315 in the Wuchaba pluton (1) have the same magmatic mineralogy as the host and a fine-grained  
316 texture without any disequilibrium features such as crystal resorption or reactive overgrowth  
317 (Fig. 3d), which, together with lacking metamorphic or residual sedimentary fabrics, rules out  
318 the restite origin; (2) the similar U-Pb ages of both MMEs and the host (e.g., Zhu et al. 2013)  
319 also argue against the restite model; (3) the MMEs have greater amphibole modes with  
320 cumulate texture formed by hornblende-plagioclase; (4) MMEs have slightly higher  $\epsilon_{\text{Nd}}(t)$  or

321  $\epsilon_{\text{Hf}}(t)$  than their host granitoids and have similar Sr isotopes (Fig. 12). The similar isotope  
322 variation ranges for both granitoid hosts and the MMEs are inconsistent with mafic-felsic  
323 magma mixing, but are consistent with the same mantle source with varying extents of crustal  
324 contamination as discussed above (Figs. 11-12).

325 Many authors still follow the popular view that the similar Sr-Nd-Hf isotope between the  
326 host and MMEs have resulted from magma mixing. We emphasize that it is physically unlikely  
327 that isotopes become homogenized whereas major and trace elements are not (Niu et al. 2013;  
328 Chen et al. 2015). It also should be noted that the MMEs and host rocks have significant linear  
329 trends in  $\text{SiO}_2$  variation diagrams (Fig. 8), which could be interpreted as magma mixing, but  
330 they are more consistent with fractional crystallization with superimposed/enhanced effects of  
331 modal mineralogy. It is important to note that the fine grain size of MMEs is no evidence  
332 against their cumulate origin, but evidences a cumulate origin at an early stage of magma  
333 cooling when magma was emplaced in a new and relatively cold ambient crust; the first major  
334 liquidus phases are amphibole ( $\pm$  biotite  $\pm$  plagioclase) and rapid quenching will facilitate  
335 abundant nucleation without between-nuclei space for growth, thus forming fine-grained MME  
336 cumulates (Chen et al. 2015). Therefore, we maintain that the MMEs represent disturbed earlier  
337 cumulate of the same magmatic system.

### 338 *Geodynamic Implications*

339 The Qinling orogenic belt culminated with the collision of the Yangtze Block (YB) with the  
340 North China Craton (NCC) in the Mid-Late Triassic along the Mianlue suture zone (Chen et al.  
341 2000, 2010; Liu et al. 2005; Jiang et al. 2010; Li et al. 2011; Dong et al. 2011, 2012, 2013,  
342 2016; Ni et al. 2012). The age data show that the NCC-YB collision occurred between 234 and



343 220 Ma (Sun et al. 2002a; Zhu et al. 2009; Qin et al. 2010; Liu et al. 2011; Dong et al. 2012;  
344 Li et al. 2013, 2015). The Luchuba and Wuchaba granitoids have identical crystallization ages  
345 to other late Triassic granitoids in the WQOB (Zhang et al. 2007). The popular explanation is  
346 that slab break off along the Qinling-Dabie orogen occurred at shallow depth causing  
347 asthenosphere upwelling and lower crust melting causing widespread Triassic granitoid  
348 magmatism (Sun et al. 2002a). However, it is physically difficult to have asthenosphere  
349 upwelling without significant mantle lithosphere delamination (removal) and lower crust  
350 melting. In fact, continuous lithosphere extension and delamination in the WQOB occurred at  
351 < 210 Ma (Yang et al. 2012). Other authors postulated a thermal pulse associated with the slab  
352 break off resulting from the asthenosphere upwelling along the Mianlue suture during the Late  
353 Triassic; the upwelling triggered partial melting of the Neoproterozoic SCLM that generated  
354 the MME and the partial melting of the Neo-Mesoproterozoic lower crust for the granitic  
355 magmatism (Qin et al. 2009; Zhu et al. 2013). The MMEs are of cumulate origin with the  
356 hornblende-plagioclase assemblage of the same magmatic system as the host granitoid rather  
357 than representing mafic magmas of SCLM origin (see Huang et al. 2014; Chen et al. 2015,  
358 2016). Hence, partial melting of Mesoproterozoic crustal rocks and melt interaction with sub-  
359 continental lithospheric mantle (SCLM) is also implausible.

360 The magma emplacement ages for the Luchuba and Wuchaba granitoids broadly coincide  
361 with the timing of the NCC-YB collision. It is remarkable that the Nb-Ta-Ti depletion and the  
362 subchondritic Nb/Ta ratio are characteristic of these granitoids without invoking active  
363 subduction-zone magmatism; subduction-related magmatism would produce variably high  
364 excess Sr that is inconsistent with the Sr deficiency of the granitoids (Fig. 9). Therefore, we

365 suggest that in the late Triassic the WQOB witnessed a period of syn-collisional granitoid  
366 magmatism not subduction-related magmatism. The following scenario is proposed to explain  
367 the petrogenesis of the Luchuba and Wuchaba granitoids.

368 We argue that the YB-NCC collision began at ~220 Ma (Fig. 15) and finished ~210 Ma  
369 (see discussion above). Upon collision, the Mianlue oceanic crust (as old as ~350 Ma; Xu et al.  
370 2002) that had been subducted beneath the Qinling active (Andean-type) continental margin  
371 (Dong et al. 2012) may have undergone melting producing the melts parental to the Luchuba  
372 and Wuchaba granitoids. It is possible and likely that the Mianlue oceanic crust reached  
373 temperatures in excess of 800 °C with continued underthrusting to produce significant amounts  
374 of melt. Because during Triassic subduction to collision hot thermal conditions prevailed at an  
375 active continental margin with a geotherm >20 °C/km well within the melting conditions  
376 (Kelemen et al. 2003). Therefore, the remaining Mianlue oceanic crust was continuously and  
377 slowly subducted along high T/P paths (as attaining thermal equilibrium with the superjacent  
378 hot active continental margin) resulting in enhanced heating at the early stage of YB-NCC  
379 collision. The underthrusting Mianlue ocean crust began to melt when passing through the  
380 hydrous basaltic/granitic solidus (<650 °C) under amphibolite facies conditions (Mo et al. 2008,  
381 Niu et al. 2013). Such conditions and processes can produce andesitic melts parental to the  
382 Luchuba and Wuchaba granitoids. It is noteworthy that we emphasized melting of MORB under  
383 amphibolite facies conditions not amphibole dehydration melting which requires much higher  
384 temperature (>850°C, Rushmer 1991). The latter can hardly produce volumetrically significant  
385 granitoids (see above). These granitoids resemble the composition of the BCC without the Y  
386 or HREE depleted “garnet signature”, in support of melting under amphibolite facies conditions

387 without garnet present as a residual phase (details see Section 3.2.3 in Niu et al. 2013). The  
388 andesitic parental magma when emplaced in a magma chamber would rapidly cool and  
389 crystallize mafic minerals (e.g., hornblende, biotite) and plagioclase to form fine-grained  
390 cumulates (MMEs), which can be readily disturbed by replenishing magmas, leading to the  
391 more mafic cumulate to becoming dispersed as MMEs in the granitoid host. Our model is  
392 consistent with open-system magma chamber processes with continued evolution (fractional  
393 crystallization)/replenishment accompanied by crustal contamination and assimilation.

#### 394 **Conclusions**

395 (1) Zircon U-Pb dating yields ages of  $211 \pm 1.4$  Ma and  $218.5 \pm 2.3$  Ma for the Luchuba pluton  
396 and of  $218.7 \pm 1.3$  Ma for the Wuchaba pluton, respectively. This is within the age range of the  
397 collision of the Yangtze Block with the North China Craton.

398 (2) The granitoids of the Luchuba and Wuchaba plutons display an enriched LILE and LREE  
399 patterns and have variable negative Eu anomalies, which is similar to, but more evolved than,  
400 those of bulk continental crust. Our results suggest that the Luchuba and Wuchaba plutons are  
401 best explained by melting of amphibolite of MORB protolith (the Paleo-Tethys Mianlue ocean  
402 crust) during continental collision, which produced granitic melts with a remarkable  
403 compositional similarity to the BCC with inherited mantle-like isotopic compositions modified  
404 by AFC process-like assimilation.

405 (3) MMEs of Wuchaba pluton are earlier cumulates of the same magmatic system.

406 (4) Ocean crust (MORB-like) contributes to the source of the Luchuba and Wuchaba granitoids,  
407 pointing to the significance of ocean crust melting in contributing to the continental crust  
408 accretion.

409

410

#### 411 **Acknowledgements**

412 We thank Cui Huixia, Gong Hongmei, Guo Pengyuan, Hu Zhenxing, Liu Jinju, Ma Yuxin, Sun  
413 Pu, Sun Wenli, Wang Xiaohong, Ye Lei, Ye Xiaolu and Zhang Guorui for assistance with  
414 sample preparation. We particularly thank Su Li for major and trace element analysis and zircon  
415 analysis and Ma Jinlong for Sr-Nd-Hf isotope analysis. This work was supported by grants  
416 from National Natural Science Foundation of China (41130314, 91014003), Chinese Academy  
417 of Sciences, regional and local authorities (Shandong Province and City of Qingdao) and  
418 Qingdao National laboratory of ocean sciences and Technology.

419

420

#### 421 **References**

- 422 Andersen T (2002) Correction of common lead in U–Pb analyses that do not report <sup>204</sup>Pb. *Chem*  
423 *Geol* 192:59–79
- 424 Bacon CR, Druitt TH (1988) Compositional evolution of the zoned calcalkaline magma  
425 chamber of Mount Mazama, Crater Lake, Oregon. *Contrib Mineral Petrol* 98:224-256
- 426 Barbarin B (2005) Mafic magmatic enclaves and mafic rocks associated with some granitoids  
427 of the central Sierra Nevada batholith, California: nature, origin, and relations with the  
428 hosts. *Lithos* 80:155-177
- 429 Beard J, Lofgren G (1991) Partial melting of basaltic and andesitic greenstones and  
430 amphibolites under dehydration melting and water-saturated conditions at 1, 3, and 6.9  
431 kilobars. *J Petrol* 32:365-401
- 432 Blichert-Toft J, Albarède F (1997) The Lu-Hf isotope geochemistry of chondrites and the  
433 evolution of the mantle-crust system. *Earth and Planetary Science Letters* 148:243-258
- 434 Cao XF, Lü XB, Yao SZ, Mei W, Zou XY, Chen C, Liu ST, Zhang P, Su YY, Zhang B (2011)  
435 LA–ICP–MS U–Pb zircon geochronology, geochemistry and kinetics of the Wenquan ore-  
436 bearing granites from West Qinling, China. *Ore Geol Rev* 3:120-131

- 437 Castillo P R (2006) An overview of adakite petrogenesis. *Chin Sci Bull* 51:257-268
- 438 Castillo P R (2012) Adakite petrogenesis. *Lithos* 134:304-316
- 439 Chappell BW, White AJR (1974) Two contrasting granite types. *Pacific Geol* 8:173-174
- 440 Chappell BW, White AJR, Williams IS, Wyborn D, Wyborn LAI (2000) Lachlan Fold Belt  
441 granites revisited: high- and low-temperature granites and their implications. *Aust J Earth*  
442 *Sci* 47:123–138
- 443 Chauvel C, Lewin E, Carpentier M, Arndt NT, Marini JC (2008) Role of recycled oceanic basalt  
444 and sediment in generating the Hf–Nd mantle array. *Nature Geoscience* 1: 64-67
- 445 Chen YD, Price RC, White AJR (1989) Inclusions in Three S-Type Granites from Southeastern  
446 Australia. *Journal of Petrology* 30:1181-1218
- 447 Chen YJ, Li C, Zhang J, Li Z, Wang HH (2000) Sr and O isotopic characteristics of porphyries  
448 in the Qinling molybdenum deposit belt and their implication to genetic mechanism and  
449 type. *Sci China Ser D* 43:82–94 (Suppl.)
- 450 Chen YJ (2010) Indosinian tectonic setting, magmatism and metallogenesis in Qinling Orogen,  
451 central China. *Geology in China* 37:854–865 (in Chinese with English abstract)
- 452 Chen S, Niu YL, Sun WL, Zhang Y, Li JY, Guo PY, Sun P (2015) On the origin of mafic  
453 magmatic enclaves (MMEs) in syn-collisional granitoids: evidence from the Baojishan  
454 pluton in the North Qilian Orogen, China, *Miner Petrol*:1-20
- 455 Chen S, Niu YL, Li JY, Sun WL, Zhang Y, Hu Y, Shao FL (2016) Syn-collisional adakitic  
456 granodiorites formed by fractional crystallization: Insights from their enclosed mafic  
457 magmatic enclaves (MMEs) in the Qumushan pluton, North Qilian Orogen at the northern  
458 margin of the Tibetan Plateau. *Lithos* 248: 455-468
- 459 Clemens JD, Stevens G (2011) What controls chemical variation in granitic magmas. *Lithos*  
460 134-135:317-329
- 461 Collins WJ, Beams SD, White AJR, Chappell BW (1982) Nature and origin of A-type granites  
462 with particular reference to southeastern Australia. *Contrib Mineral Petrol* 80:189-200
- 463 Corfu F, Hanchar JM, Hoskin PWO, Kinny P (2003) Atlas of zircon textures. *Rev Mineral*  
464 *Geochem* 53:469–500
- 465 Dahlquist J (2002) Mafic microgranular enclaves: Early segregation from metaluminous

466 magma (sierra de Chepes), Pampean Ranges, NW Argentina. *J South Am Earth Sci*  
467 15:643-655

468 Defant M J, Drummond M S (1990) Derivation of some modern arc magmas by melting of  
469 young subducted lithosphere. *Nature* 347:662-665

470 Depaolo D J (1981) Trace element and isotopic effects of combined wallrock assimilation and  
471 fractional crystallization. *Earth Planet Sci Lett* 53:189-202

472 Dong YP, Zhang GW, Neubauer F, Liu XM, Genser J, Hauzenberger C (2011) Tectonic  
473 evolution of the Qinling orogen, China: review and synthesis. *J Asian Earth Sci* 41:213-  
474 237

475 Dong YP, Liu XM, Zhang GW, Chen Q, Zhang XN, Li W, Yang C (2012) Triassic diorites and  
476 granitoids in the Foping area: Constraints on the conversion from subduction to collision  
477 in the Qinling orogen, China. *J Asian Earth Sci* 47:123-142

478 Dong YP, Liu XM, Neubauer F, Zhang GW, Tao N, Zhang YG, Zhang, XN, Li W (2013) Timing  
479 of Paleozoic amalgamation between the North China and South China Blocks: evidence  
480 from detrital zircon U-Pb ages. *Tectonophysics* 586:173-191

481 Dong YP, Santosh M (2016) Tectonic architecture and multiple orogeny of the Qinling  
482 Orogenic Belt, Central China. *Gondwana Res* 29:1-40

483 Feng YM, Cao XZ, Zhang EP, Hu YX, Pan XP, Yang JL, Jia QZ, Li WM (2002) Structure,  
484 orogenic processes and geodynamic of the western Qinling orogen (in Chinese). Xi'an  
485 map press, Xi'an, pp 1-263

486 Foley SF, Barth MG, Jenner GA (2000) Rutile/melt partition coefficients for trace elements and  
487 an assessment of the influence of rutile on the trace element characteristics of subduction  
488 zone magmas. *Geochim Cosmochim Acta* 64:933-938

489 Foley S, Tiepolo M, Vannucci R (2002) Growth of early continental crust controlled by melting  
490 of amphibolite in subduction zones. *Nature* 417:837-840

491 Gao T (2011) The LA-ICP-MS zircon U-Pb dating, geology and geochemistry, tectonic setting  
492 of several important intrusions from the north part of the western stage of west Qinling  
493 and their relationship with mineralization. PhD thesis, Chang'an University, Xi'an, China

494 Hanchar JM, Hoskin PWO (2003) Zircon. *Rev Mineral Geochem* 53:1-500

495 Higuchi H, Nagasawa H (1969) Partition of trace elements between rock-forming minerals and  
496 the host volcanic rocks. *Earth Planet Sci Lett* 7:281-287

497 Huang H, Niu YL, Nowell G, Zhao ZD, Yu XH, Zhu DC, Mo XX, D S (2014) Geochemical  
498 constraints on the petrogenesis of granitoids in the East Kunlun Orogenic belt, northern  
499 Tibetan Plateau: Implications for continental crust growth through syn-collisional felsic  
500 magmatism. *Chem Geol* 370:1-18

501 Jahn BM, Wu FY, Chen B, (2000) Massive granitoid generation in central Asia: Nd isotopic  
502 evidence and implication for continental growth in the Phanerozoic. *Episodes* 23:82-92

503 Jiang YH, Jin GD, Liao SY, Zhou Q, Zhao P (2010) Geochemical and Sr-Nd-Hf isotopic  
504 constraints on the origin of Late Triassic granitoids from the Qinling orogen, central China:  
505 Implications for a continental arc to continent-continent collision. *Lithos* 117:183–197

506 Kelemen PB, Rilling JL, Parmentier E, Mehl L, Hacker BR (2003) Thermal structure due to  
507 solid-state flow in the mantle wedge beneath arcs. *Geophys Monogr Am Geophys Union*  
508 138:293-311

509 Klein M, Stosch HG, Seck H, Shimizu N, (2000) Experimental partitioning of high field  
510 strength and rare earth elements between clinopyroxene and garnet in andesitic to tonalitic  
511 systems. *Geochim Cosmochim Acta* 64:99-115

512 Li N, Chen YJ, Fletcher IR, Zeng QT (2011) Triassic mineralization with Cretaceous overprint  
513 in the Dahu Au-Mo deposit, Xiaoqinling gold province: Constraints from SHRIMP  
514 monazite U-Th–Pb geochronology. *Gondwana Res* 20:543-552

515 Li T, Xu XY, Chen JL, Wang HL, Li ZP, Zhang X (2012) LA-ICP-MS zircon U-Pb dating and  
516 tectonic setting of Zhongchuan intrusion, Lixian area, West Qinling orogen. *Geol Bull*  
517 31:875-883

518 Li XH, Liu DY, Sun M, Li WX, Liang XR, Liu Y (2004) Precise Sm–Nd and U–Pb isotopic  
519 dating of the supergiant Shizhuyuan polymetallic deposit and its host granite, SE  
520 China. *Geol Mag* 141:225-231

521 Li XH, Qi CS, Liu Y, Liang XR, Tu XL, Xie LW, Yang YH (2005) Rapid separation of Hf from  
522 rock samples for isotope analysis by MC-ICPMS: a modified single-column extraction  
523 chromatography method. *Geochimica* 34:109-114

524 Li XH, Long WG, Li QL, Liu Y, Zheng YF, Yang YH, Chamberlain KR, Wan DF, Guo CH,

- 525 Wang XC, Tao H (2010) Penglai zircon megacrysts: a potential new working reference  
526 material for microbeam determination of Hf–O isotopes and U–Pb age. *Geostand Geoanal*  
527 *Res* 34:117-134
- 528 Li XW, Mo XX, Yu XH, Ding Y, Huang XF, Wei P, He WY (2013) Petrology and  
529 geochemistry of the early Mesozoic pyroxene andesites in the Maixiu Area, West Qinling,  
530 China: products of subduction or syn-collision? *Lithos* 172/173:158–174
- 531 Li XW, Mo XX, Huang XF, Dong GC, Yu XH, Luo MF, Liu YB (2015) U–Pb zircon  
532 geochronology, geochemical and Sr–Nd–Hf isotopic compositions of the early indosinian  
533 Tongren pluton in West Qinling: petrogenesis and geodynamic implications. *J Asian Earth*  
534 *Sci* 97:38-50
- 535 Liu SF, Steel R, Zhang GW (2005) Mesozoic sedimentary basin development and tectonic  
536 implication, northern Yangtze Block, eastern China: record of continent–continent  
537 collision. *J Asian Earth Sci* 25:9-27
- 538 Liu SW, Li QG, Tian W, Wang ZQ, Yang PT, Wang W, Bai X, Guo RR (2011a) Petrogenesis  
539 of Indosinian granitoids in Middle-Segment of South Qinling Tectonic Belt: constraints  
540 from Sr–Nd isotopic systematics. *Acta Geol Sin Engl* 85:610–628
- 541 Liu SW, Yang PT, Li QG, Wang ZQ, Zhang WY, Wang W (2011b) Indosinian granitoids and  
542 orogenic processes in the middle segment of the Qinling orogen, China. *Journal of Jilin*  
543 *University (Earth science edition)*, 41(6):1928-1943
- 544 Lu Z, Quan JJ, Chen X, Yan DF (2004) Characteristics and geological effects of magmatic  
545 activity of the Zhongchuan granite of western Qinling area. *Acta Geologica Gan Su* 12:25-  
546 30
- 547 Ludwig K (2012) User's manual for Isoplot version 3.75-4.15: a geochronological toolkit for  
548 Microsoft. Excel Berkley Geochronological Center Special Publication No. 5
- 549 Mattauer M, Matte P, Malavieille J, Tapponnier P, Maluski H, Qin XZ, Qin TY (1985) Tectonics  
550 of the Qinling belt: Build-up and evolution of eastern Asia. *Nature* 317(6037): 496-500
- 551 Martin H, Smithies RH, Rapp R, Moyen JF, Champion D (2005) An overview of adakite,  
552 tonalite–trondhjemite–granodiorite (TTG), and sanukitoid: relationships and some  
553 implications for crustal evolution. *Lithos* 79:1-24
- 554 Meng QR, Zhang GW (2000) Geologic framework and tectonic evolution of the Qinling-Dabie



555 orogen, central China. *Tectonophysics* 323:183-196

556 Mo XX, Luo ZH, Deng JF, Yu XH (2007) Granitoids and crustal growth in the east-Kunlun  
557 orogenic belt. *Geological Journal of China Universities* 3:403-414 (in Chinese with  
558 English abstract)

559 Mo XX, Niu YL, Dong GC, Zhao ZD, Hou ZQ, Zhou S, Ke S (2008) Contribution of  
560 syncollisional felsic magmatism to continental crust growth: A case study of the Paleogene  
561 Linzizong volcanic succession in southern Tibet. *Chem Geol* 250:49-67

562 Ni ZY, Chen YJ, Li N, Zhang H (2012) Pb-Sr-Nd isotope constraints on the fluid source of the  
563 Dahu Au-Mo deposit in Qinling Orogen, central China, and implication for Triassic  
564 tectonic setting. *Ore Geol Rev* 46:60-67

565 Niu YL, O'Hara MJ (2009) MORB mantle hosts the missing Eu (Sr, Nb, Ta and Ti) in the  
566 continental crust: new perspectives on crustal growth, crust–mantle differentiation and  
567 chemical structure of oceanic upper mantle. *Lithos* 112:1-17

568 Niu YL, Zhao ZD, Zhu DC, Mo XX (2013) Continental collision zones are primary sites for  
569 net continental crust growth—A testable hypothesis. *Earth Sci Rev* 127:96-110

570 Ou CS, Yang YC, Wang H, Yang WG (2010) Characteristics and mineralization of Luchuba  
571 granite pluton in Lixian. *Gansu Science and Technology* 017:37-41

572 Peng X (2012) Magmatic consanguinity and tectonic significance of Zhongchuan rock group  
573 in western Qinling. MSc thesis, Chang'an University

574 Peng Xuan (2013) Research on homology for the rock group of monzonite granite in the  
575 Western Qinling. *Northwestern Geology* 1:63-80

576 Pertermann M, Hirschmann MM, Hametner K, Günther D, Schmidt MW (2004) Experimental  
577 determination of trace element partitioning between garnet and silica-rich liquid during  
578 anhydrous partial melting of MORB-like eclogite. *Geochem Geophys Geosy* 5: 297-391

579 Qin JF, Lai SC, Grapes R, Diwu CR, Ju YJ, Li YF (2009) Geochemical evidence for origin of  
580 magma mixing for the Triassic monzonitic granite and its enclaves at Mishuling in the  
581 Qinling orogen (central China). *Lithos* 112:259–276

582 Qin JF, Lai SC, Grapes R, Diwu CR, Ju YJ, Li YF (2010) Origin of Late Triassic high Mg  
583 adakitic granitoid rocks from the Dongjiangkou area, Qinling orogen, central China

584 implications for subduction of continental crust. *Lithos* 120:347-367

585 Raczek I, Jochum KP, Hofmann AW (2003) Neodymium and strontium isotope data for USGS  
586 reference materials BCR-1, BCR-2, BHVO-1, BHVO-2, AGV-1, AGV-2, GSP-1, GSP-2  
587 and eight MPI-DING reference glasses. *Geostand Newslett* 27:173-179

588 Ratschbacher L, Hacker BR, Calvert A, Webb LE, Crimmer JC, McWilliams MO, Ireland T,  
589 Dong S, Hu J (2003) Tectonics of the Qinling (Central China): tectonostratigraphy,  
590 geochronology, and deformation history. *Tectonophysics* 366:1-53

591 Rubatto D, Gebauer D (2000) Use of cathodoluminescence for U–Pb zircon dating by ion  
592 microprobe: some examples from the Western Alps. In: Pagel M, Barbin V, Blanc P,  
593 Ohnenstetter D (eds), *Cathodoluminescence in Geosciences*. Springer, Berlin, pp 373-400

594 Rushmer T (1991) Partial melting of two amphibolites: contrasting experimental results under  
595 fluid absent conditions. *Contrib Mineral Petrol* 107:41-59

596 Rudnick RL, Gao S (2003) Composition of the continental crust. *Treatise Geochem* 3:1-64

597 Schnetzler CC, Philpotts JA (1970) Partition coefficients of rare-earth elements between  
598 igneous matrix material and rock-forming mineral phenocrysts; II. *Geochim Cosmochim*  
599 *Acta* 34:331-340

600 Shen J, Zhang ZQ, Liu DY (1997) Sm–Nd, Rb–Sr,  $^{40}\text{Ar}/^{39}\text{Ar}$ ,  $^{207}\text{Pb}/^{206}\text{Pb}$  age of the Douling  
601 metamorphic complex from eastern Qinling orogenic belt. *Acta Geol Sin* 18:248-254

602 Song SG, Niu YL, Wei CJ, Ji JQ, Su L (2010a) Metamorphism, anatexis, zircon ages and  
603 tectonic evolution of the Gongshan block in the northern Indochina continent—an eastern  
604 extension of the Lhasa Block. *Lithos* 120:327-346

605 Song SG, Su L, Li XH, Zhang GB, Niu YL, Zhang LF (2010b) Tracing the 850-Ma continental  
606 flood basalts from a piece of subducted continental crust in the North Qaidam UHPM belt,  
607 NW China. *Precambrian Res* 183:805-816

608 Sun WD, Li SG, Chen YD, Li YJ (2002a) Timing of synorogenic granitoids in the South  
609 Qinling, central China: constraints on the evolution of the Qinling–Dabie orogenic belt. *J*  
610 *Geol* 110:457-468

611 Sun WD, Li SG, Sun Y, Zhang GW, Li Q (2002b) Mid-Paleozoic collision in the North Qinling:  
612 Sm–Nd, Rb–Sr and  $^{40}\text{Ar}/^{39}\text{Ar}$  ages and their tectonic implications. *J Asian Earth Sci*

613 21:69-76

614 Sun SS, McDonough WF (1989) Chemical and isotopic systematics of oceanic basalts:  
615 implications for mantle composition and processes. In: Saunders AD, Norry MJ (eds),  
616 Magmatism in the ocean basins. Geol Soc London Spec Publ 42:313-345

617 Vervoort JD, Patchett PJ, Blichert-Toft J, Albarède F (1999) Relationships between Lu-Hf and  
618 Sm-Nd isotopic systems in the global sedimentary system. Earth Planet Sci Lett 168:79-  
619 99

620 Vervoort JD, Plank T, Prytulak J (2011) The Hf-Nd isotopic composition of marine sediments.  
621 Geochim Cosmochim Acta 75:5903-5926

622 Wall VJ, Clemens JD, Clarke DB (1987) Models for granitoid evolution and source  
623 compositions. J Geol 95:731-749

624 Wang F, Lu XX, Lo CH, Wu FY, He HY, Yang LK, Zhu RX (2007) Post-collisional, potassic  
625 monzonite–minette complex (Shahewan) in the Qinling Mountains (central China):  
626  $^{40}\text{Ar}/^{39}\text{Ar}$  thermochronology, petrogenesis, and implications for the dynamic setting of the  
627 Qinling orogen. J Asian Earth Sci 31:153-166

628 Wang XX, Wang T, Castro A, Pedreira R, Lu XX, Xiao QH (2011) Triassic granitoids of the  
629 Qinling orogen, central China: genetic relationship of enclaves and rapakivi-textured  
630 rocks. Lithos 2011:369-387

631 Wang XX, Wang T, Zhang CL (2015) Granitoid magmatism in the Qinling orogen, central  
632 China and its bearing on orogenic evolution. Sci China Earth Sci 58:1497-1512

633 Wang YL, Zhang CQ, Wang CH, Hou KJ (2012) Hf isotopic composition of the Qinjia granites  
634 from the Debao Cu deposit, Guangxi: Implications for crust - mantle interaction.  
635 Geotectonica et Metallogenia 36:377-383

636 Wang ZQ, Yan QR, Yan Z, Wang T, Jiang CF, Gao LD, Liu P (2009) The new division of the  
637 main tectonic unit for the Qinling orogenic belt. J Geol 83:1527-1546

638 Wei GJ, Liang XR, Li XH, Liu Y (2002) Precise measurement of Sr isotopic composition of  
639 liquid and solid base using (LP) MC-ICPMS. Geochimica 31:295-305

640 Whalen JB (1985) Geochemistry of an Island-Arc Plutonic Suite: the Uasilau-Yau Yau  
641 Intrusive Complex, New Britain, P.N.G. J Petrol 26:603-632

- 642 Wiedenbeck M, Alle P, Corfu F, et al. (1995) Three natural zircon standards for U - Th - Pb,  
643 Lu - Hf, trace element and REE analyses. *Geostandards Newslett* 19:1-23
- 644 Wu FY, Jahn BM, Wilde SA, Lo CH, Yui TF, Lin Q, Ge WC, Sun DY (2003) Highly  
645 fractionated I-type granites in NE China: geochronology and petrogenesis. *Lithos* 66:241-  
646 273
- 647 Wu YB, Zheng YF (2012) Tectonic evolution of a composite collision orogen: an overview on  
648 the Qinling–Tongbai–Hong'an–Dabie–Sulu orogenic belt in central China. *Gondwana Res*  
649 23:1402-1428
- 650 Xiao B, Li QG, Liu SW, Wang ZQ, Yang PT, Chen JL, Xu XY (2013) Highly fractionated Late  
651 Triassic I-type granites and related molybdenum mineralization in the Qinling orogenic  
652 belt: Geochemical and U–Pb–Hf and Re–Os isotope constraints. *Ore Geol Rev* 56:220-  
653 233
- 654 Xing FM, Xu X (1996) AFC mixing model and origin of intrusive rocks from Tongling area.  
655 *Acta Petrologica et Mineralogica* 15:10-15
- 656 Xu JF, Castillo PR, Li XH, Zhang BR, Han YW (2002) MORB-type rocks from the Paleo-  
657 Tethyan Mian-Lueyang northern ophiolite in the Qinling mountains, central China:  
658 Implications for the source of the low  $^{206}\text{Pb}/^{204}\text{Pb}$  and high  $^{143}\text{Nd}/^{144}\text{Nd}$  mantle component  
659 in the Indian ocean. *Earth Planet Sci Lett* 198:323-337
- 660 Xu XY, Li T, Chen JL, Li P (2013) The granitoids magmatism and mineralization in west  
661 section of the western Qinling, NW China. *Northwest geology* 5:76-82
- 662 Xu XY, Chen JL, Gao T, Li P, Li T (2014) Granitoid magmatism and tectonic evolution in  
663 northern edge of the West Qinling terrance, NW China. *Acta Petrol Sin* 30:371-389 (in  
664 Chinese with English abstract)
- 665 Yang JS, Wu FY, Wilde S, Liu X (2007) Petrogenesis of late Triassic granitoids and their  
666 enclaves with implications for post-collisional lithospheric thinning of the Liaodong  
667 Peninsula, North China Craton. *Chem Geol* 242:155-175
- 668 Yang PT, Liu SW, Li QG, Zhang F, Wang ZQ, Wang DS, Wang RT, Yan QR, Yan Z (2011) Ages  
669 of the Laocheng granitoids and crustal growth in the South Qinling tectonic domain,  
670 Central China: zircon U–Pb and Lu–Hf isotopic constraints. *Acta Geol Sin Engl* 85:854-

671  
672  
673  
674  
675  
676  
677  
678  
679  
680  
681  
682  
683  
684  
685  
686  
687  
688  
689  
690  
691  
692  
693  
694  
695  
696  
697  
698  
699

Yang PT, Liu SW, Li QG, Wang ZQ, Wang RT, Wang W (2012) Geochemistry and zircon U–Pb–Hf isotopic systematics of the Ningshan granitoid batholith, middle segment of the South Qinling belt, Central China: constraints on petrogenesis and geodynamic processes. *J Asian Earth Sci* 61:166-186

Zhang CL, Zhang GW, Yan YX, Wang Y (2005) Origin and dynamic significance of Guangtoushan granitic plutons to the north of Mianlue zone in southern Qinling. *Acta Petrol Sin* 21:711-720 (in Chinese with English abstract)

Zhang GW, Zhang BR, Yuan XC, Xiao QH (2001) Qinling orogen belt and continental geodynamics. Science Press, Beijing, pp 1–729 (in Chinese)

Zhang HF, Jin LL, Zhang L, Nigel H, Zhou L, Hu SH, Zhang BR (2007) Geochemical and Pb–Sr–Nd isotopic compositions of granitoids from western Qinling belt: Constraints on basement nature and tectonic affinity. *Science in China Series D: Earth Sciences* 50:184-196

Zeng Q, McCuaig TC, Hart CJ, Jourdan F, Muhling J, Bagas L (2012) Structural and geochronological studies on the Liba goldfield of the West Qinling Orogen, Central China. *Miner Deposita* 7:799-819

Zeng Q, Mccuaig TC, Tohver E, Bagas L, Lu Y (2014) Episodic Triassic magmatism in the western south Qinling orogen, central China, and its implications. *Geol J* 49:402–423

Zhu LM, Ding ZJ, Yao SZ, Zhang WG, Song SG, Qu WJ, Guo B, Li B (2009) Ore forming event and geodynamic setting of molybdenum deposit at Wenquan in Gansu Province, Western Qinling. *Chinese Sci Bull* 54:2309-2324

Zhu LM, Zhang GW, Chen YJ, Ding ZJ, Guo B, Wang F, Lee B (2011) Zircon U–Pb ages and geochemistry of the Wenquan Mo-bearing granitoids in West Qinling, China: Constraints on the geodynamic setting for the newly discovered Wenquan Mo deposit. *Ore Geol Rev* 39:46-62

Zhu LM, Zhang GW, Yang T, Wang F, Gong HJ (2013) Geochronology, petrogenesis and tectonic implications of the Zhongchuan granitic pluton in the Western Qinling metallogenic belt, China. *Geol J* 48:310-334

700 **Figure captions**

701 **Fig. 1. (a), (b)** Simplified geological map of the western Qinling Orogenic belt (modified  
702 from Zhang et al. 2007). In (c) I = fine grained porphyritic tourmaline-bearing biotite  
703 monzonitic granite; II = fine grained porphyritic biotite monzonitic granite; III = medium-fine  
704 grained biotite monzonitic granite; IV = medium-fine grained granodiorite; V = medium  
705 grained biotite monzonitic granite; VI = porphyritic biotite monzonitic granite; VII =  
706 porphyritic monzonitic granite; and VIII = medium to fine grained biotite monzonitic granite.

707 **Fig. 2. (a)** Outcrop of Luchuba granitoid pluton with mafic magmatic enclaves (MMEs).  
708 **(b)** Outcrop of Wuchaba granitoid pluton with MMEs.

709 **Fig. 3.** Photomicrographs of Luchuba and Wuchaba plutons. **(a)** Sample SEB12-01 and  
710 **(b)** Sample YDB12-05 of Luchuba (cross-polarized light or XPL) pluton; **(c)** Sample DPC12-  
711 01 and **(d)** Sample MK12-04 of Wuchaba (XPL) pluton. **(e)** showing the sharp contact of  
712 MMEs with their host granodiorite, and MMEs are finer-grained than the host. **(f)** Sample  
713 MK12-04 of Wuchaba (PPL) pluton. The abbreviations are as follows: Pl - plagioclase, Qz -  
714 quartz, Bt - biotite, Hb - hornblende, Kfs - K-feldspar, Ap - apatite, Zr - zircon.

715 **Fig. 4.** Cathodoluminescence (CL) images of zircons from representative samples **(a)**  
716 SEB12-01 and **(b)** YDB12-05 of Luchuba pluton; **(c)** DPC12-01 of Wuchaba pluton. Red  
717 circles show analyzed spots.

718 **Fig. 5.** Zircon U–Pb concordia plots and weighted mean  $^{206}\text{Pb}/^{238}\text{U}$  ages for **(a)** SEB12-  
719 01 and **(b)** YDB12-05 of Luchuba pluton, and **(c)** DPC12-01 of Wuchaba pluton.

720 **Fig. 6.** Total alkalis ( $\text{Na}_2\text{O} + \text{K}_2\text{O}$ ) versus  $\text{SiO}_2$  (TAS) diagram showing the compositional  
721 variation of Luchuba and Wuchaba samples. The MMEs are less felsic than the hosts.

722 **Fig. 7.** Diagram of A/NK [ $\text{Al}_2\text{O}_3/(\text{Na}_2\text{O} + \text{K}_2\text{O})$ ] vs. A/CNK [molar ratio  $\text{Al}_2\text{O}_3/(\text{CaO} + \text{Na}_2\text{O}$   
723  $+ \text{K}_2\text{O})$ ] for granitoids of Luchuba and Wuchaba plutons in WQOB.

724 **Fig. 8.**  $\text{SiO}_2$  variation diagrams of representative major elements (wt.%) and selected trace  
725 elements (ppm) of Luchuba and Wuchaba samples.

726 **Fig. 9.** (a) Chondrite normalized REE patterns, and (b) Primitive mantle normalized  
727 incompatible element patterns of samples from Luchuba pluton; (c) Chondrite normalized REE  
728 patterns, and (d) Primitive mantle normalized incompatible element patterns of samples from  
729 Wuchaba pluton. For comparison, the average bulk continental crust (BCC, red solid line)  
730 (Rudnick and Gao 2003) is also plotted. Chondrite and primitive mantle values are from Sun  
731 and McDonough (1989).

732 **Fig. 10.** Plot of  $\text{Sr}/\text{Sr}^*$  vs.  $\text{Eu}/\text{Eu}^*$  for the Luchuba and Wuchaba granitoids.  $\text{Sr}/\text{Sr}^* =$   
733  $\text{Sr}_{\text{PM}}/[1/2*(\text{Pr}_{\text{PM}} \times \text{Nd}_{\text{PM}})]$ ;  $\text{Eu}/\text{Eu}^* = \text{Eu}_{\text{PM}}/[1/2*(\text{Sm}_{\text{PM}} \times \text{Gd}_{\text{PM}})]$ ; Primitive mantle values are  
734 from Sun and McDonough (1989).

735 **Fig. 11.** (a) Plot of  $I_{\text{Sr}}$  vs.  $1/\text{Sr}$  for the Luchuba and Wuchaba granitoids. (b) Plot of  $\epsilon_{\text{Nd}}(t)$   
736 vs.  $1/\text{Nd}$  for the Luchuba and Wuchaba granitoids.

737 **Fig. 12.** Plots of Sr, Nd and Hf isotopes (in the forms of initial  $^{87}\text{Sr}/^{86}\text{Sr}$  or  $I_{\text{Sr}}$ ,  $\epsilon_{\text{Nd}}(t)$  and  
738  $\epsilon_{\text{Hf}}(t)$ ) against MgO and  $\text{SiO}_2$ .

739 **Fig. 13. (a)**  $\epsilon_{\text{Nd}}(t)$  vs.  $I_{\text{Sr}}$  plot of the Luchuba and Wuchaba granitoids (modified after Qin  
740 et al. 2009); the data for the Triassic granites in western Qinling are from Zhang et al. (2007).  
741 **(b)**  $\epsilon_{\text{Nd}}(t)$  vs.  $\epsilon_{\text{Hf}}(t)$  plot. The field for crust-mantle array is from Vervoort et al. (1999) and the  
742 terrestrial array is from Vervoort et al. (2011). **(c)** Age (Ma) vs.  $\epsilon_{\text{Hf}}(t)$  plot of the Luchuba and  
743 Wuchaba granitoids, together with the literature Hf isotope data (Zhu et al. 2013).

744 **Fig. 14.** Plot of  $\epsilon_{\text{Nd}}(t)$  vs.  $\epsilon_{\text{Hf}}(t)$  for Luchuba and Wuchaba granitoids. The modeled AFC  
745 path uses parental magma (Mianlue MORB) with 6.5 ppm Nd ( $\epsilon_{\text{Nd}}(t)$ : 8.71) and 1.87 ppm Hf  
746 ( $\epsilon_{\text{Hf}}(t)$ : 16.7) (Xu et al. 2002) and a mature continental crust with 26 ppm Nd ( $\epsilon_{\text{Nd}}(t)$ : -14.5) and  
747 5.8 ppm Hf ( $\epsilon_{\text{Hf}}(t)$ : -16.8) (Shen et al. 1997) for conceptual simplicity. The Hf isotope  
748 composition for MORB is inferred from Nd isotope according to the equation ( $\epsilon_{\text{Hf}} = 1.59\epsilon_{\text{Nd}} +$   
749 1.28) given by (Chauvel et al. 2008), for continental crust according to the equation ( $\epsilon_{\text{Hf}} =$   
750  $1.36\epsilon_{\text{Nd}} + 2.95$ ) given by (Vervoort et al. 1999). AFC path calculated according to (DePaolo et  
751 al. 1981) equation. The ratio of assimilation to fractionation was set at  $r = 0.5$ . Bulk  $K_d$ 's for  
752 Nd and Hf were 0.4 and 0.6, respectively. The partition coefficients of Nd and Hf for amphibole  
753 and plagioclase are from Bacon and Druitt (1988) and for biotite from Schnetzler and Philpotts  
754 (1970) and Higuchi and Nagasawa (1969).

755 **Fig. 15.** Proposed tectonic model for the generation of the Luchuba and Wuchaba  
756 granitoids in West Qinling during the late Triassic (~220Ma). See text for explanation.



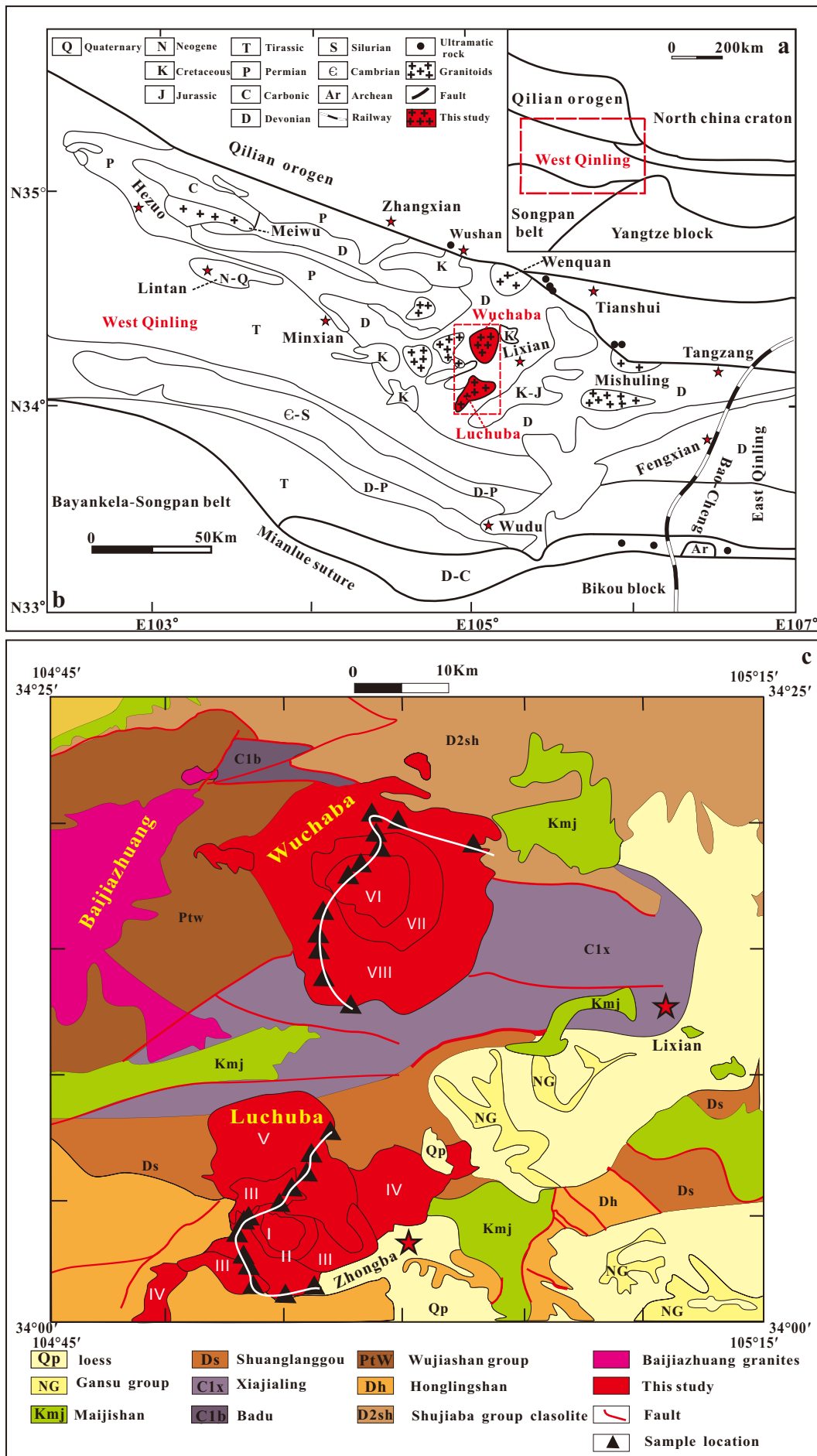


Fig.1

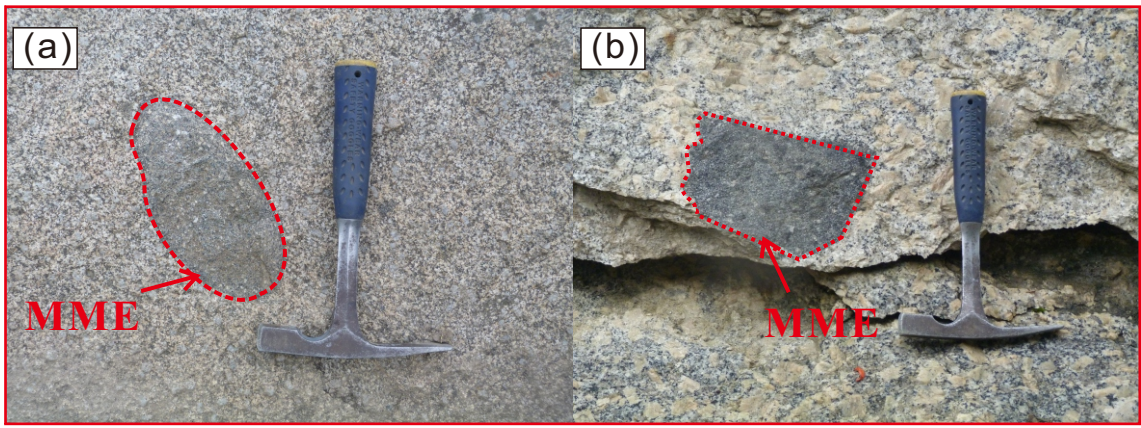


Fig.2

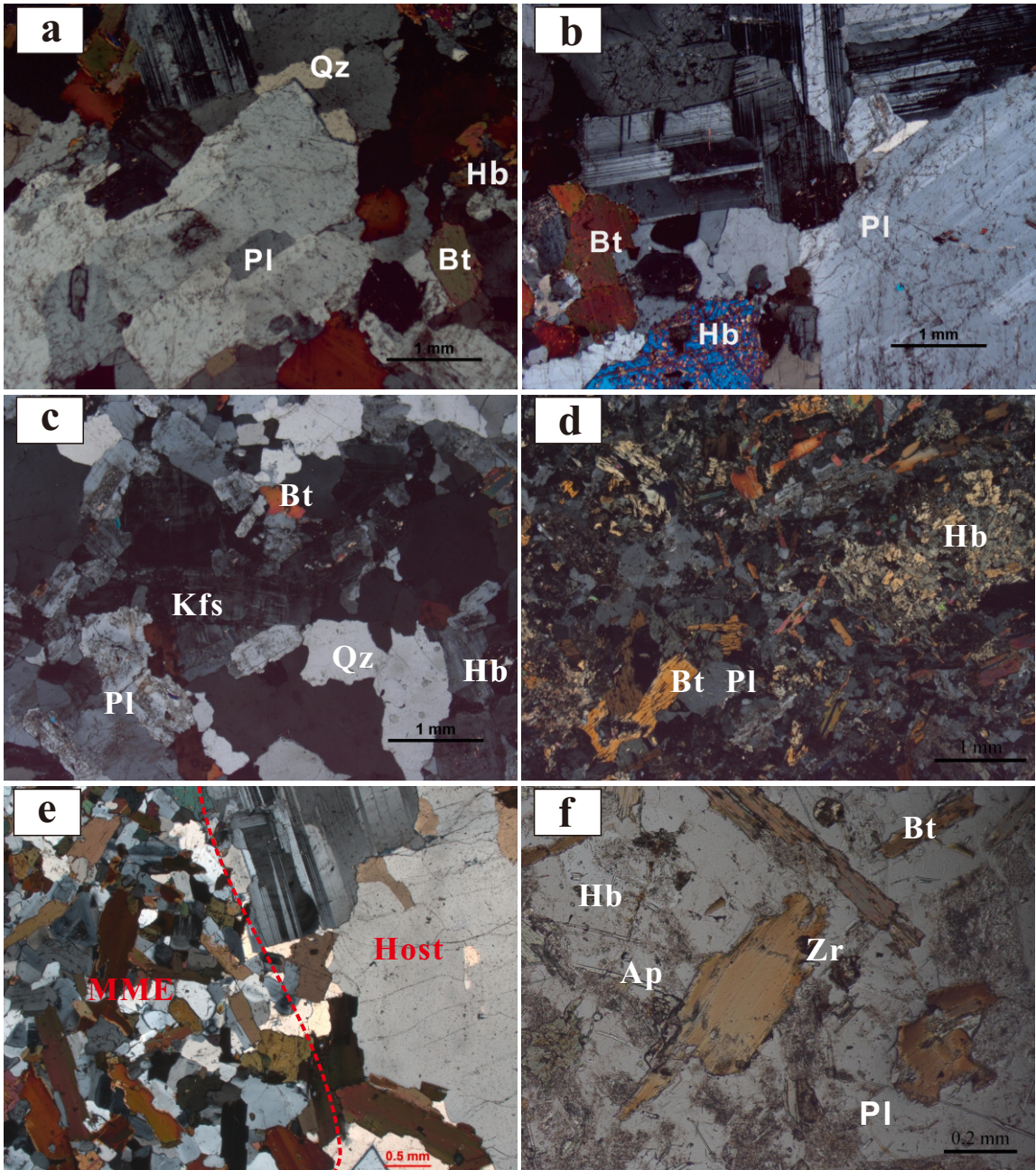
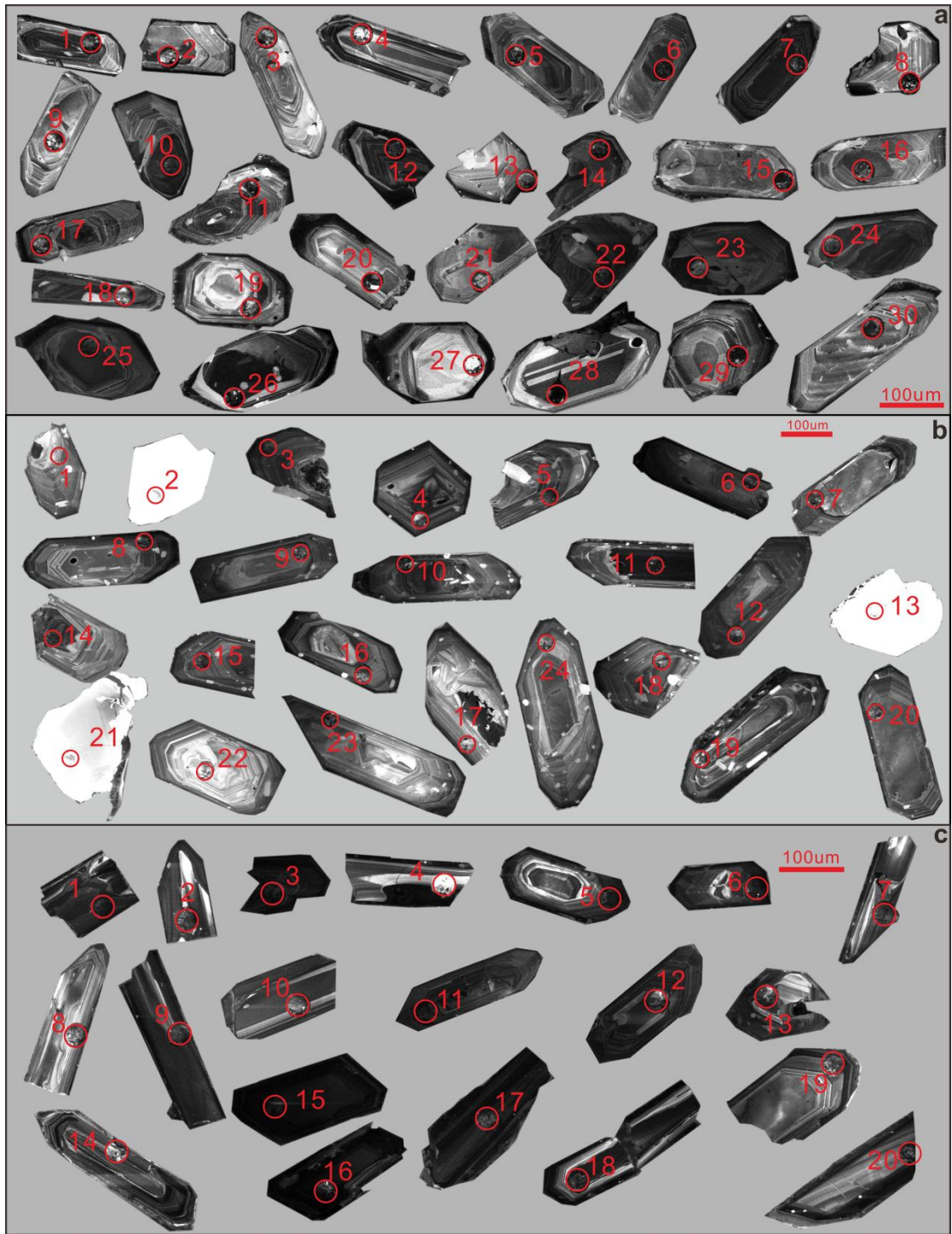


Fig.3



**Fig.4**

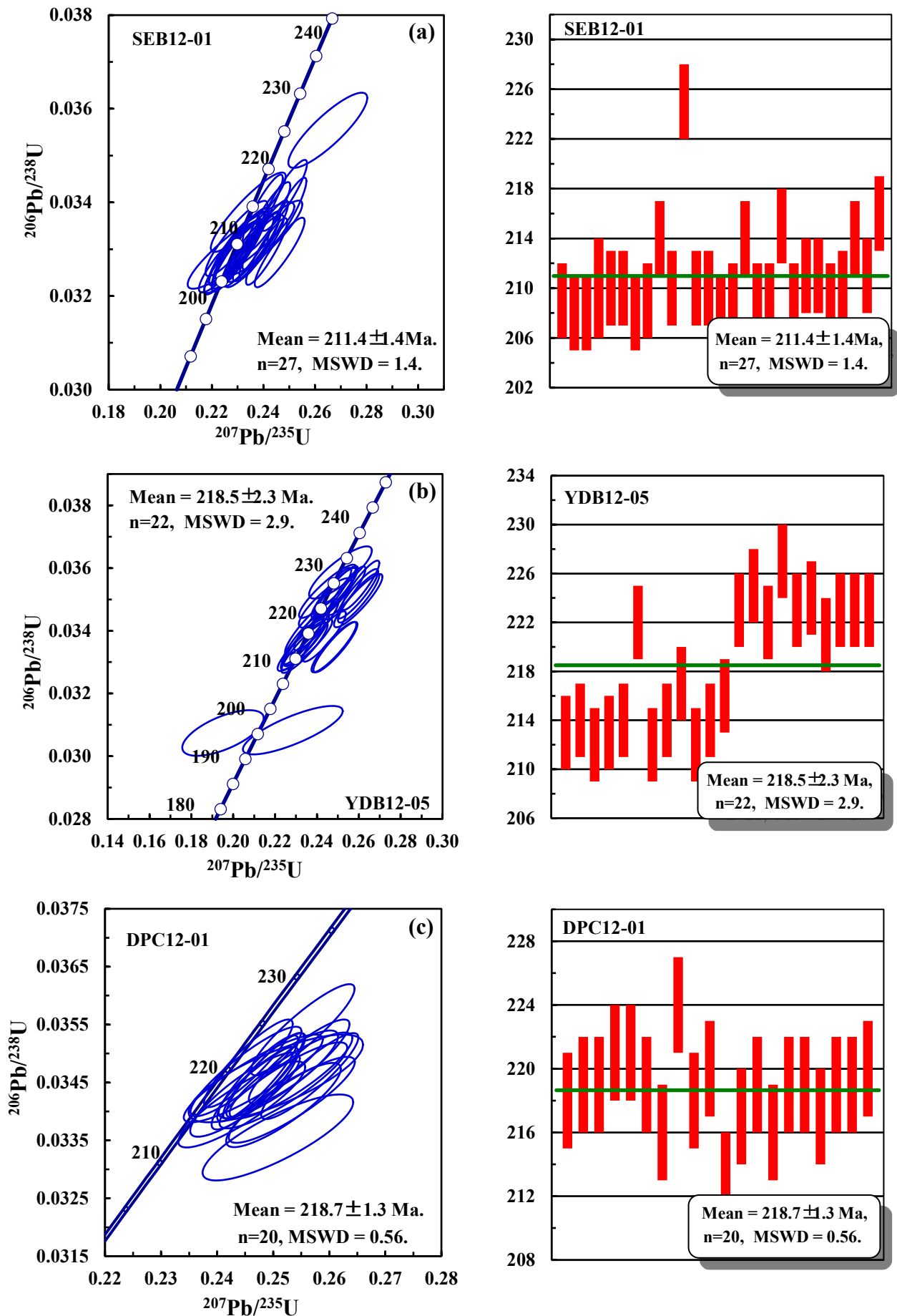


Fig.5

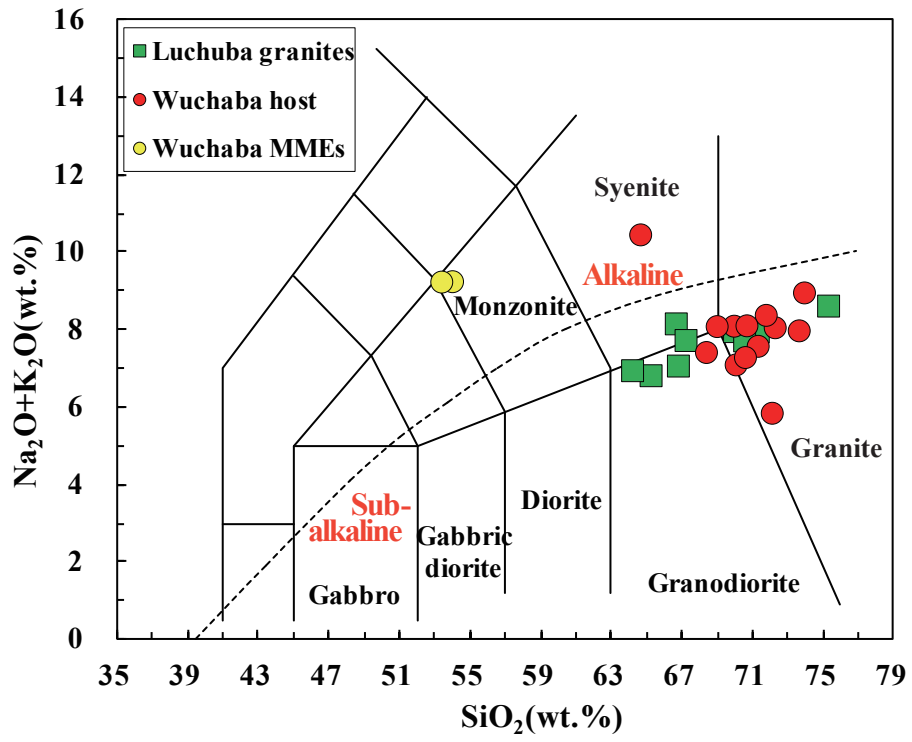


Fig.6

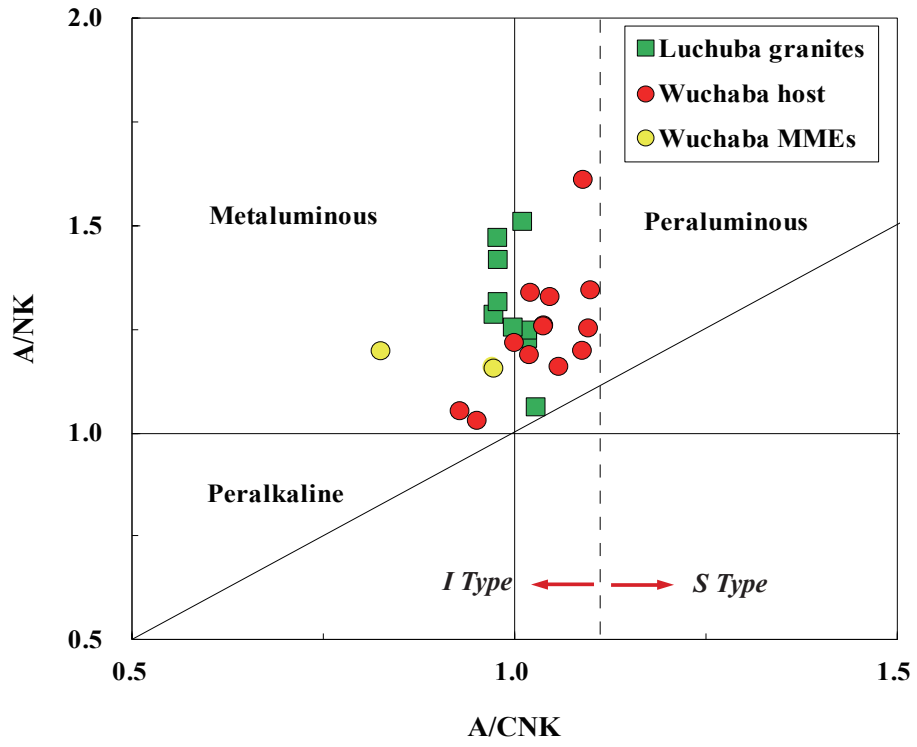


Fig.7

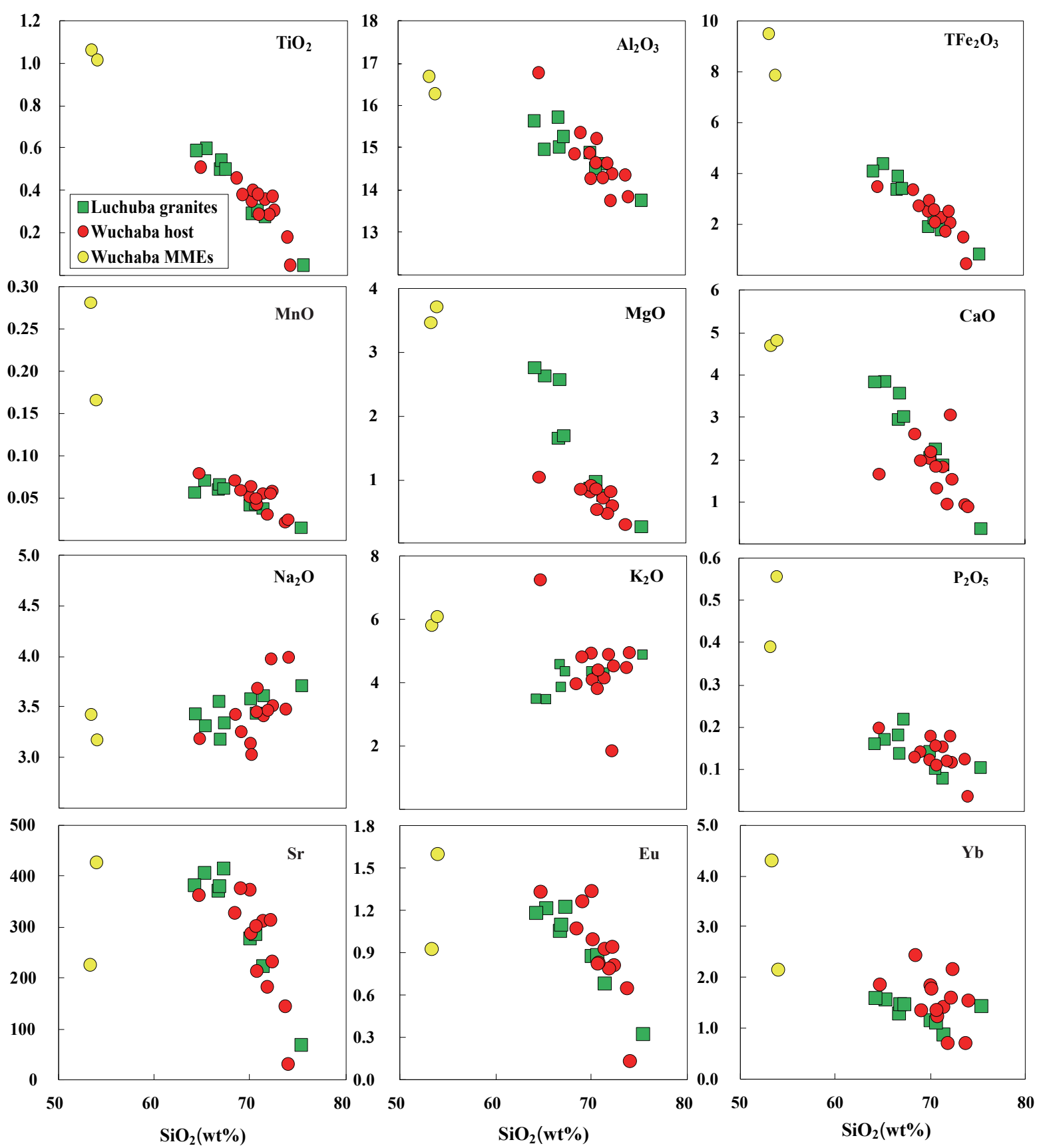


Fig.8

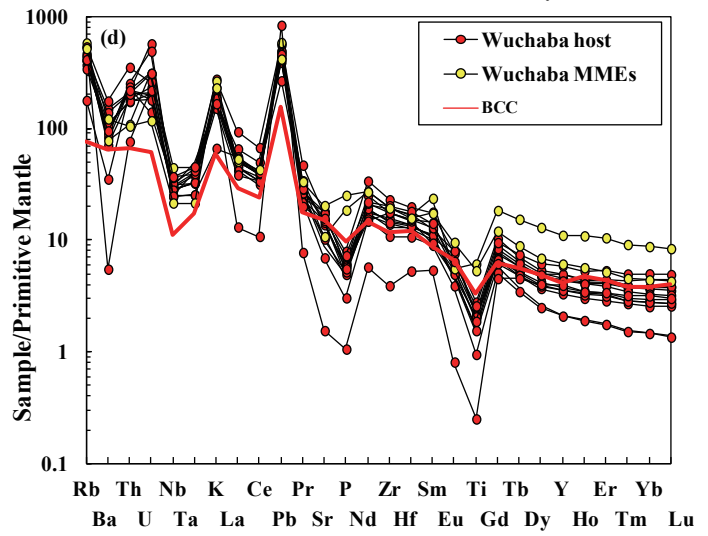
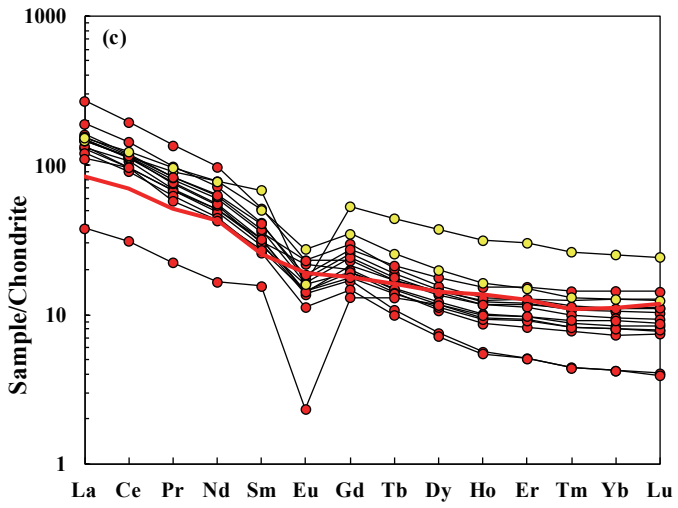
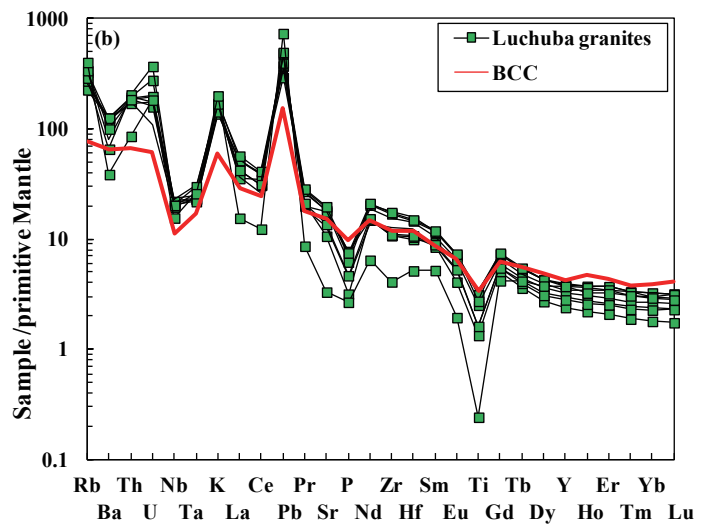
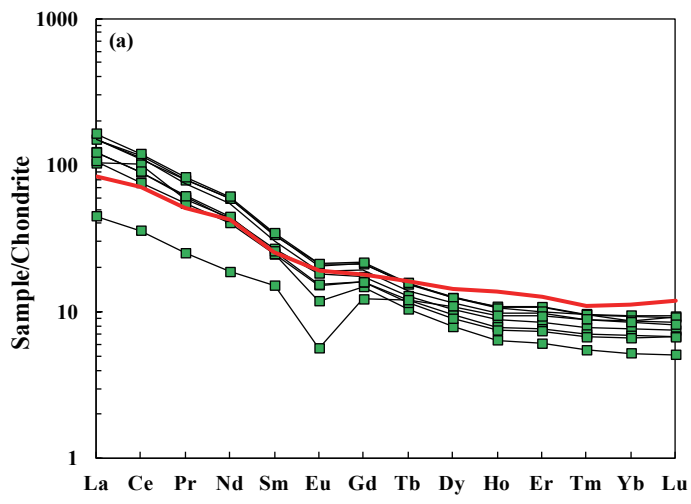


Fig.9



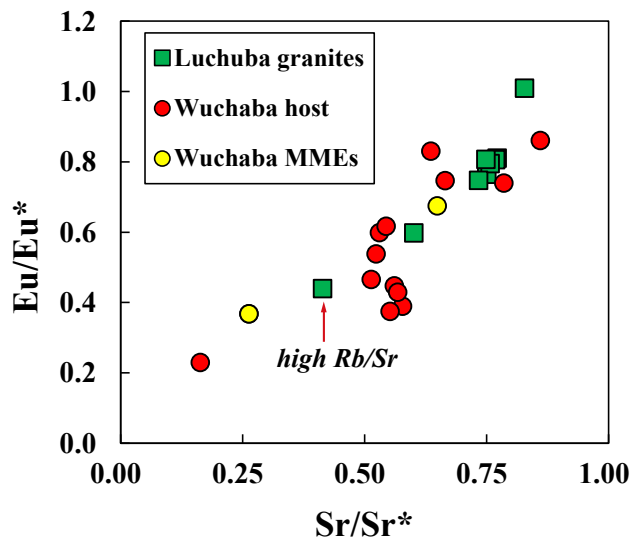


Fig.10

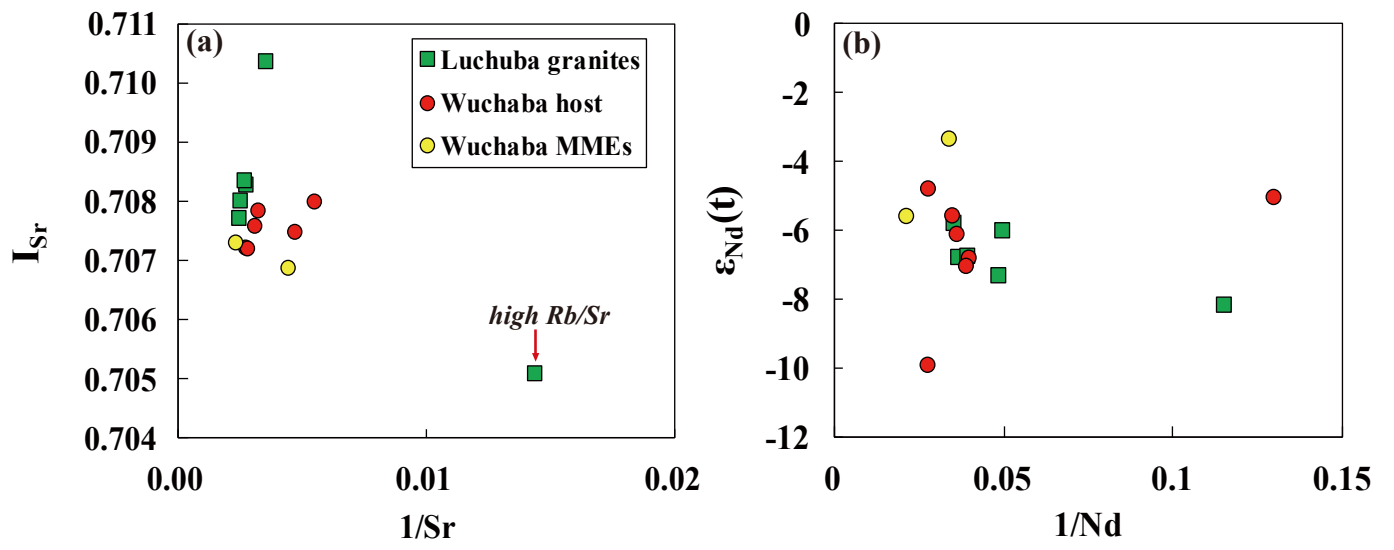


Fig.11

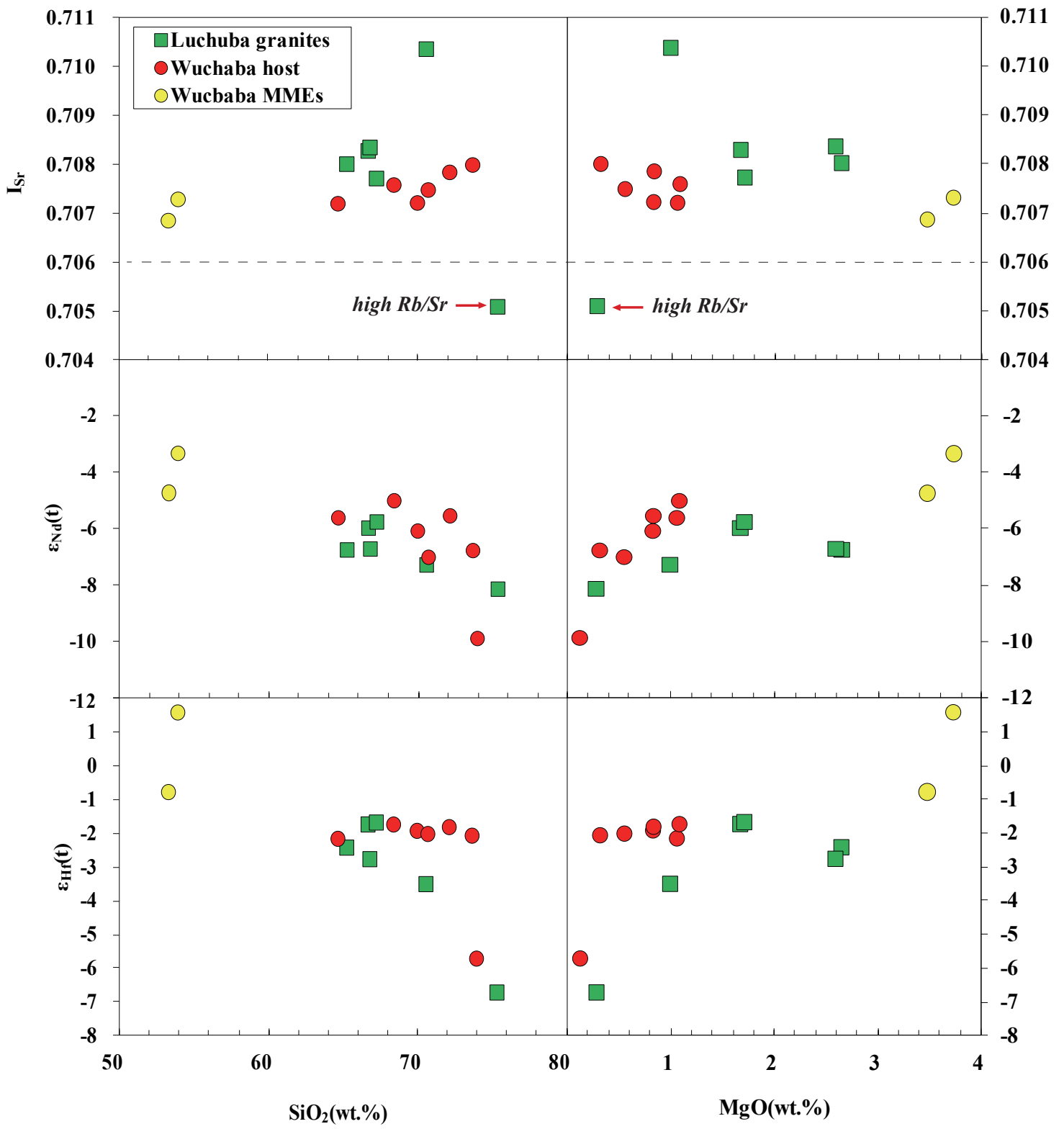


Fig.12

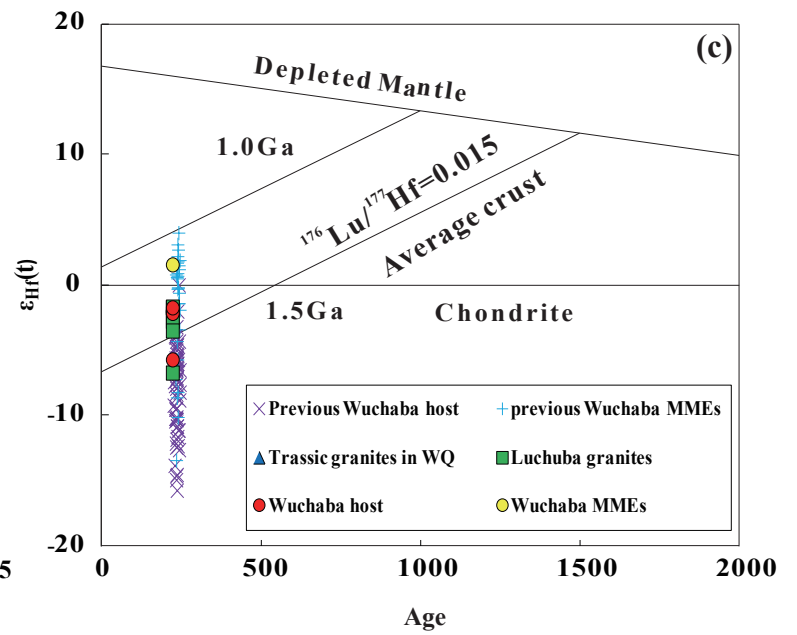
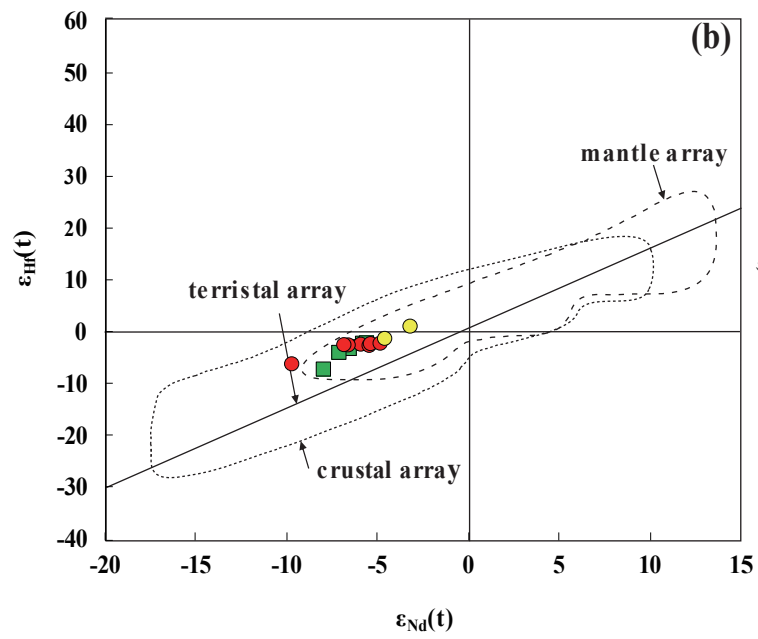
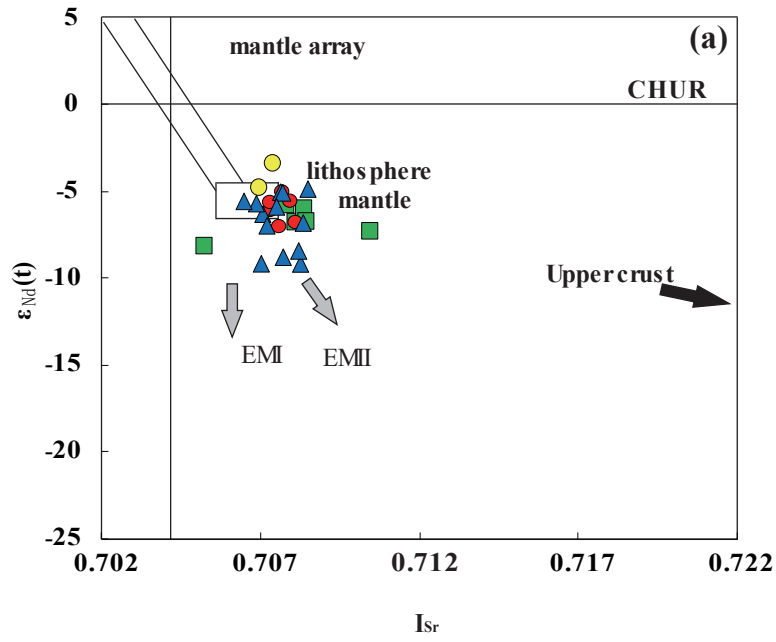


Fig.13

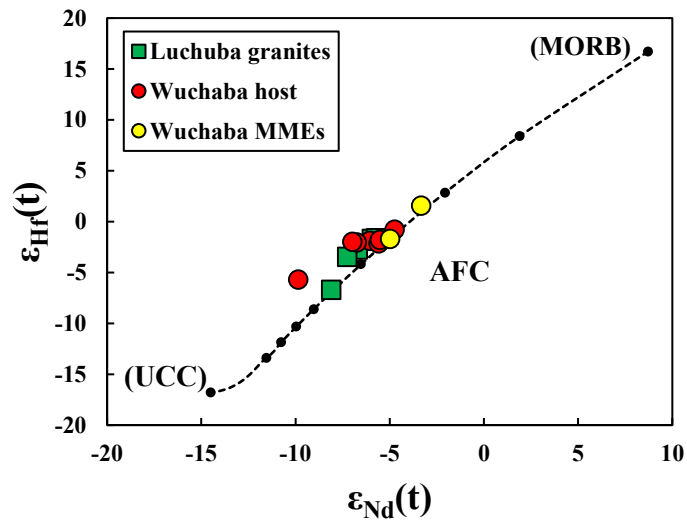


Fig.14

~Late Trassic (220Ma)

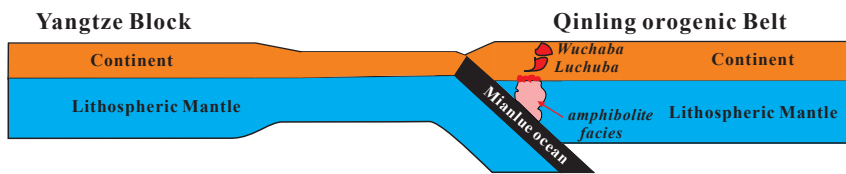


Fig.15

Table 1 Zircon U–Pb data for the Luchuba and Wuchaba pluton.

No.	Element ( ppm )			Th/U	Isotope ratio						Apparent age(Ma)					
	Pb*	U	Th		<sup>207</sup> Pb/ <sup>206</sup> Pb	1	<sup>207</sup> Pb/ <sup>235</sup> U	1	<sup>206</sup> Pb/ <sup>238</sup> U	1	<sup>207</sup> Pb/ <sup>206</sup> Pb	1	<sup>207</sup> Pb/ <sup>235</sup> U	1	<sup>206</sup> Pb/ <sup>238</sup> U	1
Sample SEB12-01(Luchuba Pluton)																
SEB-1	19.7	559	261	0.47	0.0543	0.0014	0.2463	0.0064	0.0329	0.0005	381	32	224	5	209	3
SEB-2	16.1	459	183	0.40	0.0505	0.0016	0.2284	0.0074	0.0328	0.0005	216	47	209	6	208	3
SEB-3	16.4	441	269	0.61	0.0502	0.0018	0.2273	0.0081	0.0329	0.0005	202	54	208	7	208	3
SEB-4	6.4	175	105	0.60	0.0507	0.0030	0.2313	0.0137	0.0331	0.0006	227	102	211	11	210	4
SEB-5	18.1	517	174	0.34	0.0507	0.0014	0.2315	0.0068	0.0331	0.0005	227	40	211	6	210	3
SEB-6	21.7	568	400	0.70	0.0518	0.0014	0.2361	0.0067	0.0330	0.0005	277	38	215	5	210	3
SEB-7	18.5	525	211	0.40	0.0503	0.0015	0.2273	0.0068	0.0328	0.0005	208	42	208	6	208	3
SEB-8	18.8	511	285	0.56	0.0507	0.0014	0.2299	0.0066	0.0329	0.0005	226	39	210	5	209	3
SEB-9	31.4	914	191	0.21	0.0520	0.0012	0.2418	0.0057	0.0337	0.0005	287	29	220	5	214	3
SEB-10	13.9	389	164	0.42	0.0587	0.0019	0.2674	0.0086	0.0330	0.0005	557	44	241	7	209	3
SEB-11	18.0	223	182	0.81	0.0547	0.0017	0.5114	0.0159	0.0677	0.0010	402	43	419	11	423	6
SEB-12	15.7	445	164	0.37	0.0506	0.0014	0.2307	0.0067	0.0331	0.0005	224	40	211	6	210	3
SEB-13	28.2	796	298	0.37	0.0523	0.0011	0.2385	0.0052	0.0331	0.0005	297	25	217	4	210	3
SEB-14	19.1	486	149	0.31	0.0541	0.0022	0.2650	0.0101	0.0355	0.0005	374	95	239	8	225	3
SEB-15	15.7	446	154	0.35	0.0508	0.0015	0.2318	0.0069	0.0331	0.0005	230	41	212	6	210	3
SEB-16	20.0	571	215	0.38	0.0507	0.0014	0.2295	0.0063	0.0328	0.0005	226	37	210	5	208	3
SEB-17	21.6	624	189	0.30	0.0515	0.0014	0.2340	0.0066	0.0330	0.0005	262	38	213	5	209	3
SEB-18	56.7	1655	281	0.17	0.0535	0.0010	0.2491	0.0050	0.0338	0.0005	348	22	226	4	214	3
SEB-19	36.4	1087	250	0.23	0.0531	0.0011	0.2412	0.0053	0.0330	0.0005	333	25	219	4	209	3
SEB-20	24.9	728	190	0.26	0.0502	0.0014	0.2283	0.0064	0.0330	0.0005	204	38	209	5	209	3
SEB-21	46.5	1336	306	0.23	0.0514	0.0010	0.2397	0.0051	0.0339	0.0005	257	25	218	4	215	3

(continued)

SEB-22	22.8	625	336	0.54	0.0503	0.0014	0.2288	0.0065	0.0330	0.0005	209	39	209	5	209	3
SEB-23	15.1	423	172	0.41	0.0525	0.0021	0.2408	0.0095	0.0333	0.0005	308	61	219	8	211	3
SEB-24	42.1	1219	301	0.25	0.0524	0.0012	0.2407	0.0058	0.0333	0.0005	304	30	219	5	211	3
SEB-25	21.2	597	224	0.38	0.0520	0.0016	0.2365	0.0075	0.0330	0.0005	286	45	216	6	209	3
SEB-26	29.4	867	186	0.21	0.0521	0.0013	0.2374	0.0061	0.0331	0.0005	288	32	216	5	210	3
SEB-27	12.5	360	77	0.21	0.0502	0.0021	0.2341	0.0096	0.0338	0.0006	206	64	214	8	214	3
SEB-28	15.4	419	135	0.32	0.0501	0.0017	0.2296	0.0079	0.0332	0.0005	200	51	210	7	211	3
SEB-29	24.3	525	435	0.83	0.0980	0.0043	0.4712	0.0192	0.0349	0.0006	1586	84	392	13	221	4
SEB-30	37.1	1061	232	0.22	0.0527	0.0012	0.2481	0.0058	0.0342	0.0005	315	28	225	5	216	3
Sample YDB12-05(Luchuba pluton)																
YDB-1	24.8	719	136	0.19	0.0504	0.0015	0.2332	0.0069	0.0336	0.0005	213	40	213	6	213	3
YDB-2	31.8	897	223	0.25	0.0522	0.0015	0.2435	0.0068	0.0338	0.0005	295	36	221	6	214	3
YDB-3	29.1	836	186	0.22	0.0537	0.0015	0.2481	0.0071	0.0335	0.0005	360	37	225	6	212	3
YDB-4	12.4	353	84	0.24	0.0506	0.0019	0.2343	0.0086	0.0336	0.0006	224	55	214	7	213	3
YDB-5	25.7	725	198	0.27	0.0506	0.0015	0.2350	0.0071	0.0337	0.0005	220	41	214	6	214	3
YDB-6	29.6	800	212	0.27	0.0539	0.0016	0.2597	0.0076	0.0350	0.0006	366	38	234	6	222	3
YDB-7	26.2	747	185	0.25	0.0539	0.0015	0.2489	0.0069	0.0335	0.0005	366	35	226	6	212	3
YDB-8	31.1	879	207	0.24	0.0506	0.0015	0.2349	0.0070	0.0337	0.0005	220	40	214	6	214	3
YDB-9	31.4	771	159	0.21	0.0538	0.0038	0.2285	0.0158	0.0308	0.0005	360	164	209	13	196	3
YDB-10	28.4	787	209	0.27	0.0508	0.0015	0.2397	0.0070	0.0342	0.0005	233	39	218	6	217	3
YDB-11	27.3	782	187	0.24	0.0507	0.0016	0.2341	0.0073	0.0335	0.0005	228	43	214	6	212	3
YDB-12	45.7	1315	257	0.20	0.0502	0.0014	0.2334	0.0066	0.0337	0.0005	202	37	213	5	214	3
YDB-13	26.9	751	195	0.26	0.0502	0.0016	0.2360	0.0074	0.0341	0.0006	204	43	215	6	216	3
YDB-14	22.0	596	189	0.32	0.0504	0.0018	0.2451	0.0090	0.0353	0.0006	213	56	223	7	223	3
YDB-15	63.9	1718	805	0.47	0.0534	0.0011	0.2609	0.0059	0.0355	0.0005	344	26	235	5	225	3

(continued)



YDB-16	36.9	1009	266	0.26	0.0538	0.0013	0.2599	0.0065	0.0351	0.0005	361	31	235	5	222	3
YDB-17	22.1	586	136	0.23	0.0508	0.0022	0.2513	0.0099	0.0359	0.0006	233	100	228	8	227	3
YDB-18	29.5	805	215	0.27	0.0511	0.0014	0.2481	0.0071	0.0352	0.0005	245	38	225	6	223	3
YDB-19	42.7	883	240	0.27	0.0461	0.0031	0.1952	0.0129	0.0307	0.0005		149	181	11	195	3
YDB-20	39.7	1105	229	0.21	0.0523	0.0011	0.2543	0.0059	0.0353	0.0005	298	28	230	5	224	3
YDB-21	33.4	915	209	0.23	0.0507	0.0019	0.2439	0.0083	0.0349	0.0005	227	88	222	7	221	3
YDB-22	31.4	842	305	0.36	0.0535	0.0013	0.2594	0.0065	0.0352	0.0005	349	31	234	5	223	3
YDB-23	30.5	844	193	0.23	0.0510	0.0012	0.2474	0.0059	0.0352	0.0005	239	29	224	5	223	3
YDB-24	19.4	523	157	0.30	0.0513	0.0013	0.2495	0.0067	0.0353	0.0005	255	35	226	5	223	3
Sample DPC12-01(Wuchaba pluton)																
DPC-1	80.6	2330	169	0.07	0.0520	0.0013	0.2467	0.0051	0.0344	0.0005	286	58	224	4	218	3
DPC-2	37.8	998	424	0.43	0.0517	0.0019	0.2465	0.0082	0.0346	0.0005	272	85	224	7	219	3
DPC-3	43.7	1251	208	0.17	0.0519	0.0009	0.2472	0.0048	0.0346	0.0005	279	21	224	4	219	3
DPC-4	38.4	1123	65	0.06	0.0511	0.0010	0.2456	0.0052	0.0348	0.0005	247	25	223	4	221	3
DPC-5	61.6	1719	269	0.16	0.0530	0.0014	0.2546	0.0059	0.0349	0.0005	328	63	230	5	221	3
DPC-6	76.6	2200	306	0.14	0.0521	0.0009	0.2486	0.0046	0.0346	0.0005	288	20	225	4	219	3
DPC-7	48.9	1363	184	0.14	0.0536	0.0016	0.2518	0.0068	0.0341	0.0005	352	70	228	5	216	3
DPC-8	36.0	1006	157	0.16	0.0523	0.0012	0.2553	0.0061	0.0354	0.0005	298	29	231	5	224	3
DPC-9	34.5	949	247	0.26	0.0530	0.0018	0.2518	0.0075	0.0345	0.0005	329	77	228	6	218	3
DPC-10	23.0	603	295	0.49	0.0513	0.0013	0.2451	0.0065	0.0347	0.0005	252	35	223	5	220	3
DPC-11	65.0	1677	321	0.19	0.0542	0.0021	0.2508	0.0089	0.0336	0.0005	381	88	227	7	213	3
DPC-12	29.8	829	204	0.25	0.0537	0.0018	0.2533	0.0074	0.0342	0.0005	359	75	229	6	217	3
DPC-13	29.5	826	170	0.21	0.0537	0.0011	0.2565	0.0057	0.0346	0.0005	360	26	232	5	219	3
DPC-14	39.0	1074	244	0.23	0.0520	0.0018	0.2444	0.0075	0.0341	0.0005	283	79	222	6	216	3
DPC-15	76.4	1867	212	0.11	0.0526	0.0023	0.2505	0.0103	0.0346	0.0005	310	102	227	8	219	3

(continued)

---

<b>DPC-16</b>	<b>51.8</b>	<b>1434</b>	<b>239</b>	<b>0.17</b>	<b>0.0530</b>	<b>0.0017</b>	<b>0.2532</b>	<b>0.0072</b>	<b>0.0346</b>	<b>0.0005</b>	<b>331</b>	<b>74</b>	<b>229</b>	<b>6</b>	<b>219</b>	<b>3</b>
<b>DPC-17</b>	<b>61.9</b>	<b>1732</b>	<b>210</b>	<b>0.12</b>	<b>0.0518</b>	<b>0.0016</b>	<b>0.2450</b>	<b>0.0065</b>	<b>0.0343</b>	<b>0.0005</b>	<b>277</b>	<b>70</b>	<b>222</b>	<b>5</b>	<b>217</b>	<b>3</b>
<b>DPC-18</b>	<b>50.0</b>	<b>1384</b>	<b>232</b>	<b>0.17</b>	<b>0.0529</b>	<b>0.0016</b>	<b>0.2518</b>	<b>0.0068</b>	<b>0.0345</b>	<b>0.0005</b>	<b>323</b>	<b>71</b>	<b>228</b>	<b>6</b>	<b>219</b>	<b>3</b>
<b>DPC-19</b>	<b>58.1</b>	<b>1684</b>	<b>176</b>	<b>0.10</b>	<b>0.0520</b>	<b>0.0009</b>	<b>0.2484</b>	<b>0.0048</b>	<b>0.0346</b>	<b>0.0005</b>	<b>287</b>	<b>21</b>	<b>225</b>	<b>4</b>	<b>219</b>	<b>3</b>
<b>DPC-20</b>	<b>24.9</b>	<b>714</b>	<b>78</b>	<b>0.11</b>	<b>0.0525</b>	<b>0.0017</b>	<b>0.2509</b>	<b>0.0070</b>	<b>0.0346</b>	<b>0.0005</b>	<b>309</b>	<b>74</b>	<b>227</b>	<b>6</b>	<b>220</b>	<b>3</b>

---

Table 2 Major (wt.%) and trace element concentrations (ppm) of the Luchuba and Wuchaba pluton.

Sample	Luchuba pluton						Wuchaba pluton					
	SEB12-01	SEB12-02	BSB12-01	YDB12-03	YDB12-05	NSC12-01	TJZ12-01	LTB12-01	ZKL12-01	DBQ12-01	DBQ12-03	ZTC12-01
Major elements (wt.%)												
SiO <sub>2</sub>	65.20	64.15	66.63	66.75	67.18	71.29	69.94	70.51	75.28	69.92	70.03	68.95
TiO <sub>2</sub>	0.60	0.59	0.50	0.55	0.50	0.28	0.30	0.31	0.05	0.35	0.40	0.38
Al <sub>2</sub> O <sub>3</sub>	14.98	15.66	15.74	15.04	15.28	14.64	14.91	14.53	13.78	14.90	14.29	15.38
TFe <sub>2</sub> O <sub>3</sub>	4.41	4.12	3.40	3.92	3.44	1.81	1.93	2.28	0.85	2.54	2.97	2.76
MnO	0.07	0.06	0.06	0.07	0.06	0.04	0.04	0.04	0.02	0.05	0.06	0.06
MgO	2.64	2.77	1.66	2.58	1.70	0.77	0.88	0.99	0.27	0.82	0.92	0.86
CaO	3.86	3.85	2.96	3.58	3.03	1.89	2.07	2.27	0.39	2.04	2.20	1.99
Na <sub>2</sub> O	3.32	3.44	3.56	3.19	3.35	3.62	3.59	3.44	3.72	3.15	3.04	3.26
K <sub>2</sub> O	3.51	3.52	4.61	3.89	4.39	4.35	4.39	4.28	4.91	4.96	4.12	4.84
P <sub>2</sub> O <sub>5</sub>	0.17	0.16	0.18	0.14	0.22	0.08	0.14	0.10	0.11	0.12	0.18	0.14
LOI	0.66	1.34	0.43	0.87	0.74	0.87	0.74	0.44	0.56	0.38	0.85	0.73
Na <sub>2</sub> O+K <sub>2</sub> O	6.83	6.96	8.17	7.08	7.74	7.96	7.97	7.73	8.63	8.11	7.16	8.10
K <sub>2</sub> O/Na <sub>2</sub> O	1.06	1.02	1.29	1.22	1.31	1.20	1.22	1.24	1.32	1.58	1.36	1.48
A/CNK	0.97	1.01	0.97	0.98	0.98	1.01	1.01	1.00	1.03	1.00	1.04	1.04
Total	99.43	99.66	99.75	100.58	99.90	99.63	98.92	99.20	99.93	99.24	99.08	99.36
Trace elements (ppm)												
Li	68.8	18.7	87.1	80.4	78.0	104	121	110	22.9	83.9	90.5	80.4
P	657	590	736	699	713	302	430	443	255	571	588	562
K	36140	34200	41520	44800	42580	35760	40580	42140	49860	57740	42360	50540
Sc	10.4	10.1	7.03	10.2	8.08	3.54	5.26	4.93	2.96	5.33	6.17	5.74
Ti	4368	4080	3276	4448	3558	1742	2080	2108	316	2846	2916	2722

(continued)

V	85.0	76.4	54.2	80.8	62.3	25.1	66.0	31.5	3.65	32.9	33.9	31.5
Cr	109	115	46.2	103	49.8	18.0	22.1	22.3	2.89	11.1	11.5	11.4
Mn	588	441	476	574	503	289	356	336	119	491	532	499
Co	12.3	10.0	7.47	11.6	8.71	3.21	3.66	4.22	0.31	4.34	4.40	4.30
Ni	26.4	34.1	11.2	24.5	13.3	5.63	7.97	6.05	1.24	3.26	3.54	3.57
Cu	11.4	3.79	4.09	7.07	11.0	1.20	1.38	2.41	1.11	1.06	1.76	1.94
Zn	68.6	53.0	52.0	49.4	50.7	40.5	38.6	41.8	30.5	45.2	63.1	69.7
Ga	21.9	20.0	18.5	20.0	20.9	19.7	20.9	20.1	18.3	22.3	20.7	21.2
Rb	167	144	173	165	208	184	213	215	254	276	257	234
Sr	407	383	372	381	416	224	279	287	70.0	374	289	377
Y	17.3	17.7	14.9	15.7	17.1	10.9	13.5	12.8	17.0	20.1	20.8	16.1
Zr	198	190	121	173	196	121	140	122	45.9	214	194	173
Nb	16.5	15.1	14.0	14.1	15.7	14.5	16.0	14.4	11.1	20.1	22.0	17.9
Cs	12.8	8.92	9.58	12.6	13.5	15.9	18.5	15.9	20.0	15.7	21.7	14.8
Ba	874	879	815	834	875	458	559	697	270	1042	579	963
La	35.3	35.5	24.4	35.7	39.0	29.1	25.3	28.9	10.6	35.5	44.9	30.9
Ce	71.2	67.8	61.8	69.2	73.1	54.7	46.3	55.5	21.9	68.9	88.0	65.6
Pr	7.55	7.49	5.53	7.16	7.87	5.72	5.20	5.84	2.39	7.58	9.34	6.59
Nd	27.5	27.6	20.3	25.6	28.6	20.2	18.9	20.8	8.73	27.9	33.8	24.0
Sm	5.11	5.12	4.12	4.63	5.27	3.77	3.79	3.96	2.31	5.51	6.32	4.74
Eu	1.22	1.19	1.06	1.10	1.23	0.686	0.881	0.888	0.327	1.34	1.00	1.27
Gd	4.36	4.34	3.55	3.97	4.45	3.04	3.26	3.27	2.50	4.72	5.32	4.11
Tb	0.58	0.57	0.48	0.52	0.59	0.39	0.45	0.43	0.45	0.64	0.70	0.55
Dy	3.18	3.16	2.64	2.91	3.15	2.00	2.41	2.28	2.77	3.47	3.75	2.95
Ho	0.61	0.61	0.50	0.56	0.60	0.36	0.45	0.42	0.53	0.67	0.69	0.54

(continued)

Er	1.77	1.78	1.39	1.63	1.66	1.00	1.26	1.22	1.54	1.94	1.99	1.55
Tm	0.24	0.25	0.20	0.22	0.24	0.14	0.18	0.17	0.23	0.28	0.27	0.21
Yb	1.58	1.61	1.30	1.48	1.48	0.89	1.17	1.12	1.45	1.86	1.79	1.36
Lu	0.23	0.24	0.19	0.22	0.23	0.13	0.17	0.17	0.21	0.28	0.26	0.20
Hf	4.95	4.53	3.07	4.35	4.62	3.23	3.76	3.31	1.60	5.21	4.76	4.27
Ta	1.02	0.94	0.95	1.08	0.96	0.90	1.25	1.23	1.06	1.35	1.32	1.03
Pb	25.7	20.8	26.4	24.5	28.1	34.1	34.0	35.1	52.1	33.0	27.7	30.7
Th	15.9	14.5	15.8	14.7	16.5	17.3	16.4	15.7	7.3	17.4	21.3	17.3
U	4.20	3.68	3.33	2.30	5.79	7.74	3.70	4.13	3.84	12.0	10.3	4.31
LREEs/HREEs	4.96	4.78	4.67	5.26	5.26	6.05	4.40	5.29	1.74	4.33	5.15	4.83
Eu/Eu*	0.77	0.75	0.83	0.77	0.76	0.60	0.75	0.73	0.41	0.78	0.51	0.86
(La/Yb) <sub>N</sub>	16.07	15.85	13.46	17.27	18.84	23.55	15.57	18.47	5.281	13.72	17.98	16.25
Sr/Y	23.58	21.61	25.06	24.23	24.39	20.55	20.70	22.42	4.12	18.66	13.88	23.48
Nb/Ta	16.17	16.12	14.64	13.04	16.43	16.08	12.80	11.76	10.46	14.88	16.67	17.31
Wuchaba pluton												
Sample	XJB12-01	MDG12-01	MXB12-02	MXB12-03	DPC12-01	DBL12-01	MZG12-02	CJM12-01 (host)	CJM12-01 (MME)	CJM12-03	MK12-02	MK12-04
Major elements (wt.%)												
SiO <sub>2</sub>	72.25	71.28	71.74	73.61	70.64	70.56	64.61	72.08	53.31	73.91	68.35	53.92
TiO <sub>2</sub>	0.31	0.36	0.29	0.18	0.29	0.39	0.51	0.38	1.06	0.05	0.46	1.02
Al <sub>2</sub> O <sub>3</sub>	14.40	14.31	14.65	14.38	15.24	14.67	16.79	13.77	16.70	13.86	14.88	16.28
TFe <sub>2</sub> O <sub>3</sub>	2.09	2.30	1.75	1.52	2.11	2.60	3.51	2.54	9.52	0.48	3.39	7.89
MnO	0.06	0.06	0.03	0.02	0.04	0.05	0.08	0.06	0.28	0.03	0.07	0.17
MgO	0.60	0.73	0.48	0.31	0.54	0.87	1.05	0.83	3.48	0.12	1.08	3.73
CaO	1.55	1.84	0.97	0.96	1.34	1.85	1.67	3.07	4.69	0.90	2.62	4.81

(continued)

Na <sub>2</sub> O	3.52	3.42	3.47	3.48	3.69	3.46	3.19	3.98	3.43	4.00	3.43	3.17
K <sub>2</sub> O	4.55	4.18	4.92	4.50	4.43	3.84	7.27	1.88	5.82	4.97	3.99	6.09
P <sub>2</sub> O <sub>5</sub>	0.12	0.15	0.12	0.13	0.11	0.16	0.20	0.18	0.39	0.04	0.13	0.56
LOI	0.45	0.74	0.81	1.42	0.66	0.73	0.78	0.42	0.51	0.72	0.76	0.76
Na <sub>2</sub> O+K <sub>2</sub> O	8.07	7.59	8.39	7.99	8.12	7.30	10.47	5.86	9.25	8.97	7.43	9.26
K <sub>2</sub> O/Na <sub>2</sub> O	1.29	1.22	1.42	1.29	1.20	1.11	2.28	0.47	1.70	1.24	1.16	1.92
A/CNK	1.02	1.03	1.06	1.09	1.09	1.10	0.93	1.09	0.82	0.95	1.02	0.97
Total	99.91	99.37	99.24	100.52	99.10	99.17	99.68	99.18	99.18	99.07	99.16	98.39
Trace elements (ppm)												
Li	123	117	140	62.9	131	77.5	106	47.1	134	46.4	120	168
P	444	467	464	288	492	544	752	523	1753	100	687	2381
K	40940	45080	47500	46920	44060	37700	68560	16512	65860	46060	41440	57344
Sc	4.55	4.97	2.91	2.42	3.66	4.59	6.67	6.88	23.3	2.25	6.62	17.1
Ti	2126	2584	1909	1229	2006	2662	3608	2428	7912	325.2	3338	6897
V	21.5	27.1	15.9	9.25	16.1	29.6	42.3	30.3	154	1.91	40.9	161
Cr	9.88	11.5	4.86	4.60	21.3	13.7	14.8	11.9	77.1	2.58	14.8	17.5
Mn	455	484	243	178	337	396	638	439	2422	202	583	1377
Co	3.10	3.86	2.13	1.33	2.70	4.35	5.59	3.75	17.1	0.08	5.21	18.4
Ni	3.56	4.73	3.55	2.13	13.1	6.46	5.96	3.56	16.0	1.29	5.33	8.40
Cu	1.47	2.62	1.63	1.76	2.86	4.08	2.22	2.94	66.1	0.585	3.29	3.56
Zn	61.5	54.8	78.7	106	58.0	63.0	98.5	58.0	160	22.9	76.1	101
Ga	21.4	23.1	25.4	25.6	25.9	21.9	23.6	19.9	25.5	19.6	23.3	18.8
Rb	271	257	310	295	283	215	341	113	368	339	261	328
Sr	234	313	184	146	215	303	364	315	226	32.6	329	428
Y	22.3	16.9	9.48	9.46	15.0	16.1	22.4	19.6	50.0	17.9	26.8	27.7

(continued)

Zr	144	155	166	121	160	195	256	197	220	43.6	227	216
Nb	21.5	21.0	20.3	21.8	23.0	19.9	25.9	17.4	31.6	17.6	26.2	15.3
Cs	21.9	23.6	26.5	13.5	20.8	13.0	13.9	9.55	24.9	44.3	22.8	13.3
Ba	534	782	628	491	620	729	1222	245	541	38.3	661	846
La	30.6	31.8	34.6	28.6	35.6	26.2	63.8	38.1	34.8	8.96	36.9	36.3
Ce	59.2	59.4	70.0	55.9	68.6	59.4	119	73.1	69.6	19.1	71.1	75.6
Pr	6.51	6.38	7.20	5.95	7.29	5.50	12.89	7.88	8.61	2.13	7.93	9.18
Nd	23.8	22.6	25.3	20.8	25.9	19.9	45.5	28.9	36.6	7.74	29.5	36.4
Sm	4.95	4.47	4.68	3.98	4.90	4.15	7.87	5.70	10.47	2.38	6.25	7.69
Eu	0.82	0.93	0.79	0.65	0.83	0.83	1.34	0.95	0.93	0.14	1.08	1.60
Gd	4.40	3.94	3.45	3.04	3.96	3.66	6.14	4.99	10.9	2.69	5.65	7.14
Tb	0.64	0.56	0.40	0.37	0.53	0.51	0.76	0.67	1.65	0.49	0.80	0.96
Dy	3.67	3.09	1.91	1.83	2.71	2.86	3.94	3.58	9.53	2.95	4.52	5.06
Ho	0.70	0.57	0.32	0.31	0.49	0.53	0.73	0.66	1.78	0.56	0.87	0.93
Er	2.12	1.60	0.85	0.84	1.37	1.51	2.11	1.87	5.01	1.62	2.55	2.48
Tm	0.32	0.22	0.11	0.11	0.20	0.21	0.29	0.25	0.67	0.24	0.37	0.33
Yb	2.18	1.43	0.72	0.72	1.25	1.37	1.87	1.61	4.30	1.56	2.45	2.16
Lu	0.32	0.21	0.10	0.10	0.19	0.20	0.28	0.24	0.62	0.22	0.36	0.32
Hf	3.95	3.94	4.18	3.28	4.11	4.58	6.11	4.74	5.17	1.63	5.56	4.84
Ta	2.04	1.55	1.30	1.65	1.78	1.34	1.61	1.04	1.80	1.70	1.85	0.88
Pb	34.8	34.6	31.2	39.3	35.0	29.5	40.7	18.9	41.5	59.2	32.5	29.5
Th	18.4	14.7	18.7	15.6	19.8	14.9	29.8	17.1	9.2	6.5	18.5	8.88
U	3.76	4.23	4.14	4.86	2.93	3.75	5.48	6.43	6.50	4.58	6.50	2.45
LREEs/HREEs	3.43	4.40	8.22	6.91	5.57	4.30	6.49	4.63	1.90	1.44	3.45	3.55

(continued)

Eu/Eu*	0.52	0.66	0.58	0.55	0.56	0.63	0.57	0.53	0.26	0.16	0.54	0.65
(La/Yb) <sub>N</sub>	10.07	15.97	34.61	28.64	20.48	13.73	24.48	16.96	5.80	4.13	10.80	12.03
Sr/Y	10.47	18.52	19.41	15.41	14.34	18.80	16.21	16.13	4.52	1.82	12.29	15.47
Nb/Ta	10.56	13.59	15.66	13.22	12.92	14.87	16.06	16.70	17.52	10.34	14.18	17.38

A/CNK = molar Al<sub>2</sub>O<sub>3</sub>/(CaO + Na<sub>2</sub>O+K<sub>2</sub>O); A/NK = molar Al<sub>2</sub>O<sub>3</sub>/(Na<sub>2</sub>O+K<sub>2</sub>O); Eu/Eu\* = W(Eu)<sub>N</sub>/[(1/2)(W(Sm)<sub>N</sub> + W(Gd)<sub>N</sub>)]; (La/Yb)<sub>N</sub> is normalized by Chondrite, Chondrite values are from [Sun and McDonough \(1989\)](#).



Table 3 Sr, Nd, Hf isotopes of the Luchuba and Wuchaba pluton.

Sample	<sup>87</sup> Rb/ <sup>86</sup> Sr	<sup>87</sup> Sr/ <sup>86</sup> Sr	2σSE	I <sub>Sr</sub> (t)	<sup>147</sup> Sm/ <sup>144</sup> Nd	<sup>143</sup> Nd/ <sup>144</sup> Nd	2σSE	ε <sub>Nd</sub> (t)	<sup>176</sup> Lu/ <sup>177</sup> Hf	<sup>176</sup> Hf/ <sup>177</sup> Hf	2σSE	ε <sub>Hf</sub> (t)
SEB12-01	1.18	0.711734	0.000006	0.7080	0.113	0.512173	0.000003	-6.72	0.006652	0.282595	0.000005	-2.40
BSB12-01	1.33	0.712454	0.000005	0.7083	0.124	0.512228	0.000004	-5.95	0.008734	0.282623	0.000006	-1.71
YDB12-03	1.24	0.712255	0.000005	0.7084	0.110	0.512170	0.000004	-6.69	0.007063	0.282587	0.000005	-2.74
YDB12-05	1.44	0.712253	0.000006	0.7077	0.112	0.512223	0.000003	-5.73	0.007126	0.282618	0.000003	-1.65
LTB12-01	2.16	0.717152	0.000006	0.7104	0.116	0.512150	0.000004	-7.25	0.007290	0.282567	0.000006	-3.48
ZKL12-01	10.50	0.737981	0.000016	0.7051	0.161	0.512171	0.000003	-8.11	0.018453	0.282522	0.000005	-6.70
DBQ12-01	2.14	0.713920	0.000006	0.7072	0.120	0.512218	0.000009	-6.05	0.007603	0.282613	0.000007	-1.90
MXB12-02	4.85	0.723182	0.000006	0.7080	0.112	0.512171	0.000009	-6.74	0.003485	0.282592	0.000005	-2.04
DPC12-01	3.81	0.719421	0.000006	0.7075	0.115	0.512163	0.000009	-6.98	0.006547	0.282606	0.000003	-1.99
MZG12-02	2.71	0.715710	0.000017	0.7072	0.105	0.512220	0.000011	-5.59	0.006554	0.282602	0.000005	-2.13
CJM12-01(host)	1.04	0.711114	0.000008	0.7079	0.120	0.512245	0.000010	-5.52	0.007084	0.282614	0.000006	-1.79
CJM12-01(MME)	4.70	0.721585	0.000005	0.7069	0.174	0.512363	0.000008	-4.74	0.016965	0.282683	0.000006	-0.78
CJM12-03	30.07	0.785554	—	—	0.187	0.512119	0.000012	-9.86	0.019316	0.282554	0.000006	-5.69
MK12-02	2.28	0.714738	0.000005	0.7076	0.129	0.512285	0.000008	-4.98	0.009231	0.282625	0.000005	-1.71
MK12-04	2.22	0.714264	0.000006	0.7073	0.129	0.512369	0.000007	-3.34	0.009248	0.282718	0.000006	1.58

Where, t=crystallization time of zircon (~220 Ma).<sup>87</sup>Rb/<sup>86</sup>Sr, <sup>147</sup>Sm/<sup>144</sup>Nd, <sup>176</sup>Lu/<sup>177</sup>Hf ratios calculated using Rb, Sr, Sm and Nd contents, measured by ICP-MS.

(<sup>147</sup>Sm/<sup>144</sup>Nd)<sub>CHUR</sub>=0.1967, (<sup>143</sup>Nd/<sup>144</sup>Nd)<sub>CHUR</sub>=0.512638; (<sup>176</sup>Lu/<sup>177</sup>Hf)<sub>CHUR</sub>=0.0332, (<sup>176</sup>Hf/<sup>177</sup>Hf)<sub>CHUR</sub>=0.282772 (Blichert-Toft and Albarède, 1997).